C. 1

AN EXPERIMENTAL STUDY OF THE SEISMIC FORCES ON SUBMERGED STRUCTURES

by

NEIL GORDON PEGG

B.Sc., The University Of Guelph, 1981

A THESIS SUBMITTED IN PARTIAL FULFILMENT OF

THE REQUIREMENTS FOR THE DEGREE OF

MASTER OF APPLIED SCIENCE

in

THE FACULTY OF GRADUATE STUDIES

Department Of Civil Engineering

We accept this thesis as conforming

to the required standard

THE UNIVERSITY OF BRITISH COLUMBIA

August 1983

Department of Civil Engineering

The University of British Columbia
2075 Wesbrook Place
Vancouver, Canada
V6T 1W5

Date: 16 August 1983

Abstract

In this investigation, the dynamic characteristics of a submerged cylinder were determined by performing vibration tests on a model underwater. These characteristics are expressed in terms of the added mass and damping values of the cylinder. Such quantities are required in the design of offshore structures in seismic zones. Sinusoidal tests were used to determine these values as a function of excitation frequency. The frequency range was varied from 0.5 to 6.0 Hertz, which is the primary range of interest of most earthquakes. The testing was carried out in the Seismic Simulation Laboratory of the Department of Civil Engineering at the University of British Columbia.

The experimental values of added mass and damping versus frequency were compared with the values produced using potential flow theory. The experimental and theoretical results were found to agree very closely.

The theoretical added mass and damping values were then used to develop the frequency transfer function for the base shear developed in the cylinder as a result of an input acceleration record. To check the validity of this theoretically derived transfer function, the base shear was measured for a given random acceleration input and compared to the results obtained using the theoretical transfer function. The transfer function derived from Fourier transforms of the random test records, as well as the transfer function developed through sinusoidal tests were also compared to the

theoretical transfer function; the agreement was good.

This study is restricted to structures which fall into the large body or wave diffraction regime. This means that fluid separation does not occur and Laplace's equation for potential flow can be used in solving the problem with the assumption of inviscid fluid and irrotational flow. The theoretical solution used in this work contemplates complete free surface boundary conditions, which account for the production of surface waves in the physical problem. These boundary conditions are usually ignored in other studies of this problem, as they increase the difficulty of the solution.

Part of the work for this thesis involved the design and construction of testing apparatus and procedures to be employed in the studies of seismic effects on offshore structures. This aspect of the research is described in some detail.

The study reported in this thesis confirms that an existing potential theory wave diffraction program can be used to accurately determine the added mass and added damping values for application in the aseismic design of offshore structures. These parameters can then be applied to evaluate the transfer function for such systems.

Table of Contents

List of Tables

List of Figures

Acknowledgement

Upon completion of this thesis I would like to express many thanks to my wife, Deborah and parents for their endless support. I would also like to acknowledge the considerable guidance offered to me by my supervisors, Dr. S. Cherry and Dr. M. Isaacson as well as the technical staff in the Department of Civil Engineering for their efforts in bringing about these experiments.

I. INTRODUCTION

1. BACKGROUND

The subject of fluid-structure interaction has been studied for many years. The fact that structures react differently to a given loading when located in water rather than in air has been the topic of much research. Marine engineers and hydrodynamicists have examined this problem quite thoroughly, particularly as it pertains to ship design and coastal structures. More recently, structural engineers have become seriously involved in this important problem as a result of the large increase in offshore construction. Structures which pose a potential danger to the environment, such as oil rigs and storage tanks, are being built in continuously harsher locations and an accurate analysis of all forces acting on such structures is essential.

Offshore structures undergo loading as a result of waves, currents, wind, operating machinery and seismic activity. Much work has been done on evaluating wave and current loading on submerged structures, but only recently have efforts been directed to determining the forces resulting from seismic loading. Oil rigs and other offshore structures are being built or proposed for construction in increasing numbers in various seismic zones, including the east and west coasts of Canada. This has led to the need for more research into their design for this environment. The present study, which is intended as a contribution to this general problem, is concerned with evaluating the hydrodynamic forces resulting from the seismic motions of a structure in water.

These hydrodynamic forces result from the moving body having to displace and accelerate a volume of fluid in addition to its own mass, and from drag forces developed at the surface of the moving body.

The force resulting from the body having to accelerate a volume of fluid is an inertial force and is treated as an 'added mass' that is hypothetically attached to the body's own mass and is linearly proportional to the body's acceleration.

The drag force consists of form drag, which is a result of fluid separation from the body, and skin friction, which occurs between the fluid and the body surface. The drag force dissipates energy from the system and is therefore treated as a damping force. This term is generally not linearly proportional to the structure's velocity and produces a nonlinear problem. Methods of linearizing the damping and including it as an 'added damping' term are used in some cases [24,26]. Additional 'added damping', which can be taken as being linearly proportional to the velocity, comes from the structure producing waves by its motion and dissipating energy. This term is significant in some problems.

These two terms, added mass and added damping, and the manner in which they are derived from the hydrodynamic force will be discussed further in chapter two. The determination of these two dynamic characteristics for structures in water is the object of much research done in this area.

The type of force which predominates - either form drag or inertia, determines the type of solution which can be used to solve for the hydrodynamic forces. The shape of the body, viscosity of the fluid, and the relative motion between the body and the fluid, determine the amount of drag force present. The inertia force depends on the body dimensions, fluid density and frequency of the body motion.

In the study of wave forces on structures there are two separate regimes of behaviour depending on the predominant type of force [26]:

1) small body regime, and

2) large body regime.

The small body regime is one in which significant flow separation occurs and the form drag forces are large. Structures which fall into this class are those whose dimensions, shape and relative fluid-structure motion result in fluid separation. This occurs if the cross section of the structure is small in relation to the relative motion between the structure and the water. This class of problem is mainly concerned with wave loading, as the wave length may be large in relation to the body cross section. Structures with sharp edges or other abrupt changes in cross section also induce flow separation and may fall into this regime. In the solution of this problem, the nonlinear drag term is the predominant force and the analysis is performed by means of the well known Morison equation [21]:

$$F = 0.5\rho DC_d U|U| + 0.25\rho\pi D^2 C_m(dU/dt) \qquad (1.1)$$

where, F is the fluid force, ρ is the fluid density, D is the body cross section (diameter), U is the relative velocity between the structure and the fluid, C_d is the drag coefficient and C_m is the inertia coefficient. Due to the nonlinear nature of the problem and the difficulty in attaining accurate drag and inertia coefficients, which must be determined empirically, this solution is usually difficult to obtain accurately.

The large body regime is concerned with structures and relative fluid-structure motions which do not cause flow separation. In this class of problem the inertia forces predominate. Form drag is not present as there is no flow separation. Although some drag force may result from skin friction, this is usually quite small. In general, the drag term is neglected or assumed to be small and vary linearly with the velocity of the structure. Structures whose cross sections are large in relation to the relative fluid-structure motion, and whose changes in shape are smooth, such that flow separation is not induced, fall into this regime. Another designation for this class of problem is the 'diffraction regime' as the incoming wave train, having a wave length which is not too much larger than the body cross section, is interrupted and diffracted by the body [26]. In the case of a structure undergoing motions, either from earthquake or wave loading, the waves radiated by the structure motion result in energy dissipation which can be represented as an additional damping term. This damping is usually much larger than any drag damping from skin friction and is taken to be linearly proportional to the structure velocity. This energy dissipation is considered as an 'added damping' which acts in addition to the structural damping; it is dependent on the structure dimensions, total water depth and frequency of structure motion.

When flow separation does not occur, viscous effects can usually be ignored, and the resulting linear problem is expressed by Laplace's equation for potential flow with the assumption of irrotational flow. If linearized kinematic and dynamic free surface boundary conditions are included in the analysis, the added damping due to surface wave production is incorporated in the solution [4,14,19,26]. The equations and solution governing this problem are given in appendix A.

Structures which have some local flow separation may also be studied in this regime but the effect of the degree of flow separation on the solution must be considered. The large body regime is easier to analyze than the small body regime, as the hydrodynamic force and thus the added mass and damping can be evaluated theoretically using Laplace's equation for potential flow.

Most existing theoretical and experimental studies for the earthquake design of offshore structures have been performed on the class of structures which satisfy the large body 'diffraction' regime. There are two reasons for this: first, the problem can be solved analytically by potential flow theory and second, the degree of relative motion between the structure and the fluid in seismic loading is not usually very large, so that the assumption of no flow separation is valid. This will be discussed further in chapter two.

The present study is concerned with the earthquake loading problem and therefore will be restricted to structures which satisfy the large body regime.

2. REVIEW OF LITERATURE ON EXPERIMENTAL STUDIES

In 1779, Pierre Louis Gabriel Du Buat conducted some experiments on pendulums underwater [27]. He noted that their periods of motion were different from the corresponding results obtained for the same pendulums tested in air. He explained this in terms of an added mass effect acting on the pendulums. Since that time, this added mass effect has been studied for a variety of shapes and by a variety of methods.

Several experiments have been performed in which a body on a flexible support was set into free vibration in air and in water and its natural frequencies in these environments were measured [5,6,8,20,27,28]. With the assumption that the support stiffness remains constant, the two frequency values were compared and the added mass taken as the difference in the mass values calculated from the measured frequencies. Thus, if w and m represent the frequency and mass of a system respectively and the subscripts A and w their respective values in air and in water, the added mass, m_a is obtained by equating the stiffnesses in both mediums such that:

$$w_A^2 m_A = w_W^2 m_W \tag{1.2}$$

from which

$$m_W = \frac{w_A^2 m_A}{w_W^2} \tag{1.3}$$

yields the total mass in water. The added mass is then determined from:

$$m_a = m_W - m_A \tag{1.4}$$

In 1955, Stelson and Mavis [27], conducted experiments of this type. They suspended cylinders, spheres and rectangles from a flexible beam, set them into free vibration and determined added mass quantities for the first mode frequencies in the manner described above. There was good agreement between their results and those obtained from a potential flow solution.

In 1960, Clough [6] performed similar experiments on horizontally oriented cylinders, plates and rectangles. By changing the length of the flexible supports attached to these models he was able to realize a set of systems with varying first mode natural frequencies. He measured the added mass by performing tests which excited the first mode response of his models; his results also agreed closely with those predicted from potential flow theory. His testing was done by mounting a stationary water tank over a shaking table excited by a pendulum striking the edge of the table. In addition, Clough made measurements on a flexible, vertical cantilever model and evaluated the added mass corresponding to second mode vibrations by adding weights to the model in air to reproduce the same natural period as was measured underwater. He measured damping values as well in free vibration tests and found increased damping when the models were submerged. Clough also came to the important conclusion that it was unlikely that the structural vibrations resulting from seismic loading would be large enough to induce flow separation, thus enabling one to use potential flow theory in solving this problem.

In the free vibration experiments discussed above, the dependence of the added mass and damping on the actual base excitation was not considered. The excitation may vary in amplitude and frequency. In applying a potential flow solution, the added mass and damping must be independent of amplitude, since it is assumed that no flow separation occurs. This fact was checked in the present experimental study and found to be valid. However, the added mass and damping values do depend on excitation frequency [4,19,26,31]. This is because the amount of energy required to produce the surface waves caused by structural motion varies with wave frequency, which is the same as the structure's excitation frequency. The present study is concerned with exploring how these parameters vary with excitation frequency. A dimensional analysis [20,26] of the problem (see Chapter 2.3) clearly illustrates the frequency dependence of the hydrodynamic force. The problem is governed by a second order differential equation with variable coefficients, representing the frequency dependent added mass and damping terms.

In 1965, McConnell and Young [20] investigated the dependence of added mass and damping on the Stokes number, wa^2/ν, for a sphere in a bounded fluid. Here, w is the excitation frequency, a is the radius of the sphere and ν is the kinematic viscosity of the surrounding fluid. They performed harmonic tests varying both w and ν to give the added mass and damping as a function of the Stokes number. Although this study was concerned mainly with the effects of viscosity and of an enclosing fluid boundary, variables which do not apply in the present problem, it did show a significant variation in the added mass and damping with excitation frequency. These investigators illustrated that for a given fluid, at a given excitation frequency, the problem can be resolved into a second order differential equation with constant coefficients, but that if either the fluid properties or the excitation frequency are changed, the added mass and damping coefficients change also. In solving Laplace's equation for potential flow (where viscous effects are neglected), this dependence on excitation frequency is part of the solution, provided that full kinematic and dynamic free surface boundary conditions are included in the analysis. A discussion of the boundary conditions is contained in Appendix A.

Taylor and Duncan [31], developed matrices of added mass and damping for a cylinder as functions of excitation frequency. Each element of the matrix is represented by a graph of added mass or damping versus frequency corresponding to the distortion mode of the matrix element. These were derived from potential flow theory. In the dynamic analysis of underwater structures, these 'wet' matrices from the added mass and damping are added to the corresponding 'dry' matrices and regular modal analysis follows for the structure. To verify their theoretically derived matrices, the authors conducted experiments on a hinged cylinder capable of being deformed into first and second modes by a system of levers and cams. The model was excited sinusoidally by moving its top while the base was hinged to the bottom of a stationary wave tank. They concluded that their measured added mass and damping matrices were indeed a function of excitation frequency and that they agreed well with their theoretical values.

Perhaps the most extensive experimental study of the forces resulting from earthquake loading on underwater structures was carried out on the shaking table in the Earthquake Engineering Laboratory at the University of

California by Byrd in 1978 [4]. As is the case in this present study, the table used by Byrd is capable of sinusoidal and random motion from recorded earthquakes. This allows a wide range of excitation characteristics and adds a realistic aspect to the study in that the models can be tested using actual earthquake records. In Byrd's study a pool liner was placed over the table and supported by perimeter walls constructed independent of the table. A well instrumented model of a cylindrical underwater storage tank was attached to the table such that the bottom of the tank and the model underwent the same motion. The hydrodynamic forces arising from horizontal, vertical and rotational motion were measured. Byrd performed free vibration tests to determine the natural frequency of the model in air and in water and sinusoidal tests to evaluate the added mass and damping terms as well as the total hydrodynamic force as a function of excitation frequency. He compared these results to potential flow theory ignoring the free surface boundary conditions.

As discussed earlier, the ommission of full free surface boundary conditions results in the added mass and damping terms being independent of excitation frequency; they become constants for a given structure. As Byrd conducted his experiments at frequencies above 3 Hz, where the frequency dependence has been shown to be relatively insignificant [4,8], his values corresponded well with the theoretical analysis. He concluded that while frequency dependence of the added mass and damping can be important for some structure types at low frequency excitations, it was not significant for design purposes for structures whose dimensional proportions were similar to those of his model when excited over this higher frequency range. As will be discussed in a later section, the present study investigates added mass and damping for frequencies between 0.5 and 6.0 Hz. For certain structure dimensions the frequency dependence of the added mass and damping is quite significant in this lower range of frequencies.

Byrd also conducted random vibration tests and compared the experimentally measured base shear developed in his model to that obtained using the potential flow solution.

In addition to laboratory experiments, some full scale field tests on submerged structures have also been reported in the literature. Ruhl and Budhall [25], attached hydraulic actuators to an oil rig and applied sinusoidal forced vibrations to it. They measured the first few mode shapes and periods and determined the damping characteristics of the structure. This information is useful for detecting damage from future earthquakes or heavy sea states by comparing the results with those obtained from similar measurements following such events.

3. OBJECT AND SCOPE OF INVESTIGATION

The purpose of this investigation is to determine the dynamic characteristics of large offshore structures (those which classify for a Laplace regime solution) from underwater tests of a cylindrical model. Such information is required for the seismic design of prototype systems. In the process, a testing facility to study the effects of earthquakes on a variety of underwater structures was developed.

Testing was performed on a simple cylindrical structure falling into the large body, diffraction regime, which encompasses fluid-structure interaction problems where flow separation does not occur. This allows a potential flow solution to be used. This is the case for most earthquake excited motions of a submerged structure, since the ratio of displacement to cross-section is usually small.

The added mass and damping values were determined as a function of excitation frequency through a series of sinusoidal tests ranging from 0.5 to 6.0 Hz, encompassing the range of predominant frequency components found in an earthquake record. These values were then compared to added mass and damping values derived theoretically by solving Laplace's equation for potential flow by means of a wave diffraction theory computer program available in the Department of Civil Engineering at the University of British Columbia [18].

The added mass and damping values were then used to develop a transfer function between the input base acceleration and the output base shear on the cylinder. This theoretically derived transfer function is then compared to experimentally derived transfer functions from the input and output data taken from random motion and sinusoidal tests. Also, the output base shear frequency domain spectra derived from the theoretical transfer function for a given random input were compared to the output spectra measured in the random experiments.

The overall goal is to experimentally verify the use of the theoretically derived added mass and damping values in developing a transfer function for application in the aseismic design of structures submerged in water. Figure 1 outlines the work done in this study.

Some discussion of these results in comparison to other similar studies is included, particularly to the findings of Byrd [4], whose testing program also covered some aspects of the research presently under consideration.

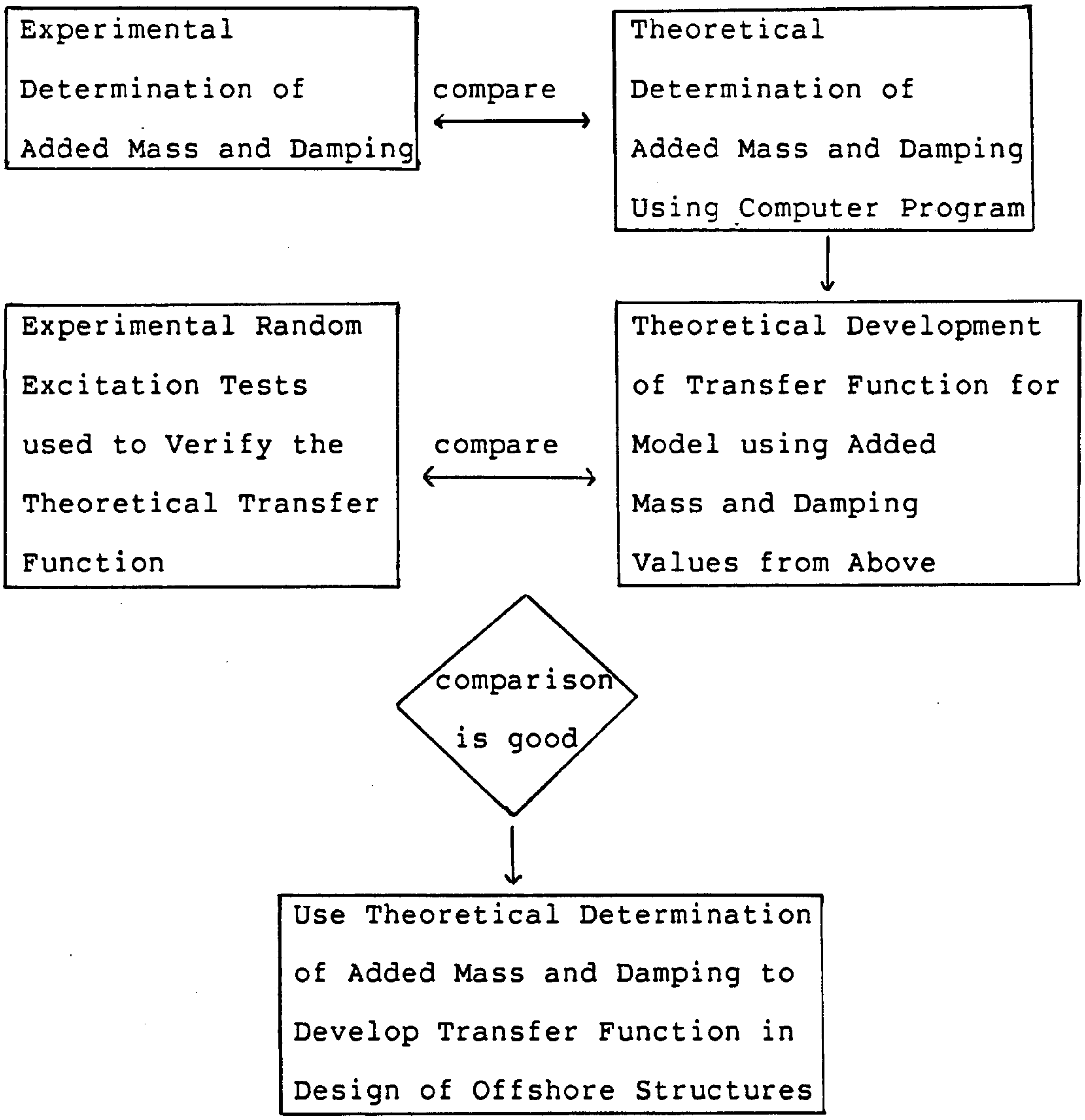

Figure 1 - Schematic of Work Performed in This Study

II. THEORY

Many analytical studies which deal with fluid forces on submerged structures have been performed. Most of these are concerned with moving fluids or waves on stationary structures. However, there are some studies which consider the structure moving in a stationary fluid; this is the situation in the case of a submerged structure excited by an earthquake [1,9,14,16,18,19,21,22,23,24,29,30,31,33,34,35].

The purpose of this chapter is: to further define the type of problem with which this study is concerned, to offer a brief review of previous theoretical work, to discuss the theoretical solution used in this study, and to develop the theory which describes how the added mass, added damping and the transfer functions may be obtained from the experimental work.

1. DEFINITION OF THE PROBLEM

The type of fluid-structure interaction problem of concern in this study is that in which no flow separation will occur. There have been several titles given to this class of problem in earlier sections of this report: large body regime, wave diffraction regime, Laplace potential flow regime and no flow separation regime. This class of problem will be referred to from here on in as the Laplace regime.

It has the following characteristics:

- the body cross section is large in relation to the relative fluid-structure motion, such that no flow separation occurs. This allows the assumption of an irrotational flow.

- the body significantly interferes with and diffracts any incoming wave train or, as in this earthquake case, if the body is near or penetrating the surface it may produce appreciable surface waves.

Laplace's equation for potential flow can be used to solve for the hydrodynamic force on a structure exhibiting the above characteristics.

A common parameter used in determining whether bodies fall into the Laplace regime is the Keulegan-Carpenter number, K defined as [26]:

$$K = \frac{2\pi A}{D} \qquad (2.1)$$

where,

A = amplitude of the relative displacement between fluid and structure,

D = structure diameter

This number determines the significance of the flow separation and viscous drag forces in a problem. If K is less than 10, inertia forces predominate over drag forces. If K is greater than 10, the drag forces are predominant and the problem moves into the small body, viscous flow regime. If K is less than 2, flow separation, and thus the drag force, is negligible. Therefore, a structure which exhibits a K value of less than 2 under either earthquake or wave loading can be studied using Laplace's equation for potential flow. Most structural motions resulting from earthquakes fall into this category, since the displacements would generally be less than 32% ($A/D<1/\pi$) of the structure's diameter.

This study pertains to relatively smooth structures having well rounded shapes. Very rough surfaces or abrupt changes in cross section may result in significant flow separation even if the body cross section is large in relation to relative fluid-structure motion.

2. ASSUMPTIONS AND CONDITIONS OF FLUID STATE

In analyzing for the hydrodynamic forces on a submerged body in the Laplace regime, the following assumptions of the fluid state are usually made:

i) No Flow Separation: Separation of the fluid from the body is prevented by ensuring that the Keulegan-Carpenter number is less than 2 as discussed in section 1 of this chapter. Any localized separation due to abrupt changes in shape or body appendages is neglected. With this situation, no significant drag forces will occur. This is also a necessary condition of the physical problem in order to make assumption ii).

ii) Irrotational Flow: This results in an ideal potential flow and allows the use of Laplace's equation for potential flow to solve the problem.

iii) Linear Wave Theory: This is also referred to as small amplitude wave theory. The wave height is assumed small in comparison to the overall water depth and wave length thus allowing the free surface boundary conditions to be linearized and applied at the still water level (appendix A), reference [26].

iv) Still Fluid: We assume that the water disturbances are due only to the structure motion; currents, waves and other outside disturbances of the water around the structure are neglected (and kept to a minimum in the experimental tests).

v) Incompressible Fluid: This assumption is valid for most studies of fluid-structure interaction. Liaw and Chopra [19] studied this topic in relation to dams and submerged towers and came to the conclusion that for most practical applications, fluid compressibility can be ignored. However, for some structure dimensions and for high frequency excitation, the energy dissipated in fluid compression waves becomes significant and fluid compressibility must be considered.

vi) Surface Wave Production: As can be seen in appendix A, ignoring surface wave radiation in the analysis simplifies the free surface boundary conditions and thus the solution of Laplace's equation. For some structures this assumption leads to good results; however, for many situations, this condition should be included, as the surface waves produced by the structure influence the value of added mass and damping. The production of surface waves by the moving body results in the existence of the added damping and in the added mass and damping both being dependent on excitation frequency [4,19,26,31]. The effect of surface waves is included in this study in both the theoretical and experimental determination of added mass and damping.

3. REVIEW OF THEORETICAL STUDIES

A brief review of existing theoretical studies pertaining to structures in the Laplace regime when excited by harmonic or random base motion is offered here. This is desirable in relation to the interpretation of the experimental data obtained in this study.

An analysis of the equation of motion (discussed in the next section), simplified by the fact that the added mass and damping are considered to be constant (independent of structure excitation), has been carried out by Penzien and

Kaul, who performed regular modal and spectral analysis on offshore towers [23]. In this analysis, the added mass and damping are simply added to the dry mass and damping of the structure. This approach appears to give results which are suitable for design approximations of some types of structures; it is used quite often in practice.

The solution of Laplace's equation for potential flow on oscillating bodies has been studied in varying degrees of complexity. The most comprehensive investigation was done by Liaw and Chopra [19], who developed a solution for a surface piercing cylinder which incorporates water compressibility and the surface waves produced by the moving structure. A simpler solution for the same problem neglecting these effects was presented by Helou and Tung [14,33]. The effect of including surface waves and water compressibility can be seen in Figure 2, taken from the work of Liaw and Chopra. Helou and Tung also extended their work to fully submerged structures. Laplace's equation, the necessary boundary conditions and the solution used in the present investigation are discussed in appendix A.

Taylor and Duncan [31], developed a design method employing added mass and damping matrices which were dependent on excitation frequency. These are derived from Laplace's equation for potential flow and are used in design with a regular modal analysis. They verified their theoretical results of these matrices by experiment.

In addition to the classical solution of Laplace's equation, studies for evaluating fluid forces have been performed using finite element techniques [16,19,22]. Although these investigations are often costly, due to the large number of equations to be solved, they are very useful in examining the response of bodies exhibiting complex geometry. Some recent studies [16] using finite elements have also included viscous effects.

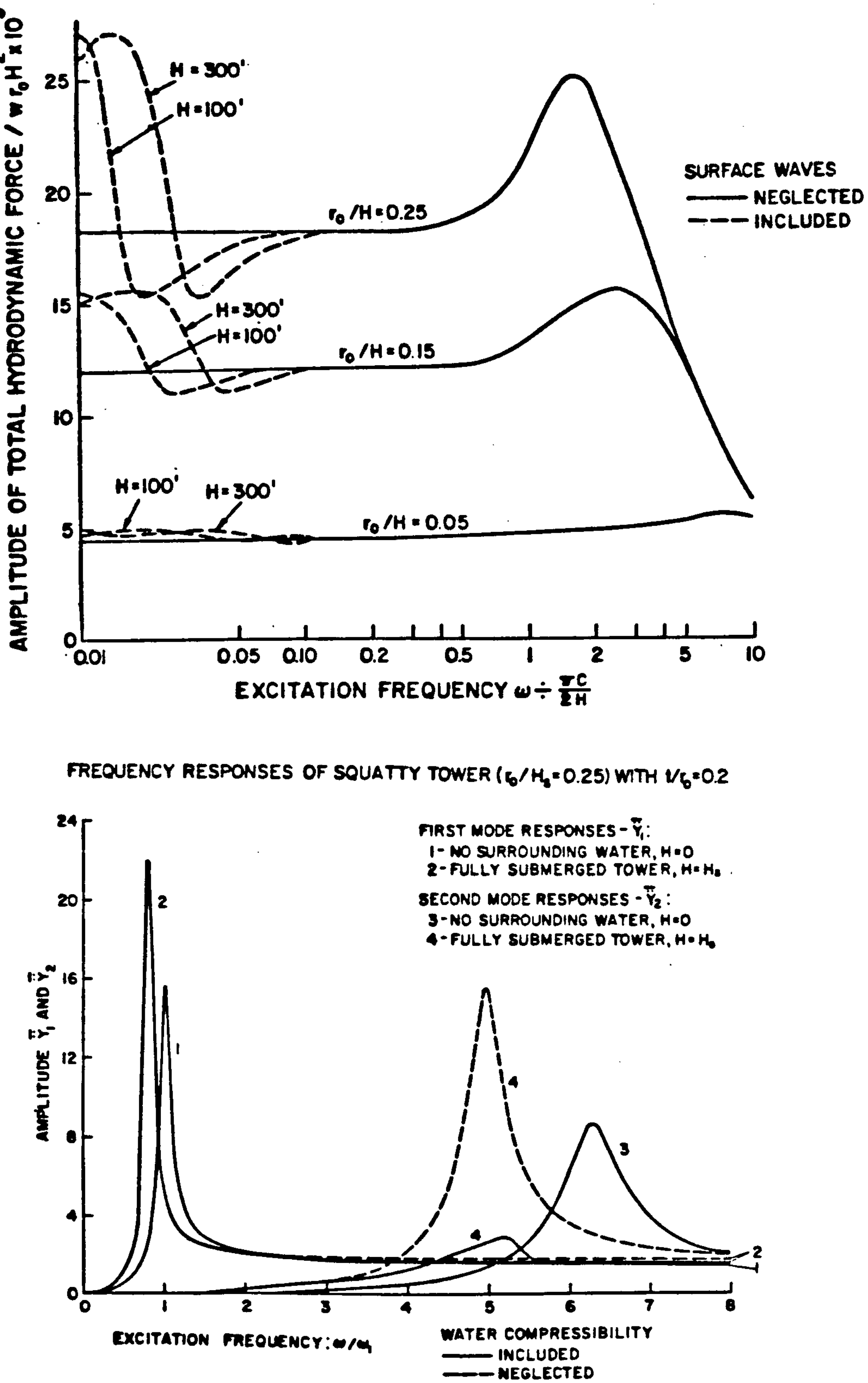

Figure 2 - Effects of Surface Waves and Compressibility from Liaw and Chopra, reference 19

4. EQUATION OF MOTION

The equation of motion for a single degree of freedom system submerged in water is developed in this section. This is usually the starting point in any study dealing with the dynamic behaviour of a system.

In general, the kinetic energy of the system gives us the inertia terms of the equation of motion. In the submerged case, the total kinetic energy is made up of the kinetic energy of the structure, T_S:

$$T_S = \frac{1}{2} m \dot{X}^2 \tag{2.2}$$

where m is the structure mass and $\dot{X}$ is the structure velocity, and the kinetic energy of the fluid, T_f:

$$T_f = \frac{1}{2} m_a \dot{X}^2 \tag{2.3}$$

where m_a is the mass of a volume of fluid set into motion by the structure. The total kinetic energy of the system T_T is then:

$$T_T = T_S + T_f = \frac{1}{2}(m + m_a)\dot{X}^2 \tag{2.4}$$

Using the Lagrange method [7] of formulating the equation of motion, we may write:

$$\frac{d}{dt}\frac{\partial T}{\partial \dot{X}} = \frac{d}{dt}(m + m_a)\dot{X} = (m + m_a)\frac{d\dot{X}}{dt} \qquad (2.5)$$

which gives the inertia term:

$$(m + m_a)\ddot{X} \qquad (2.6)$$

where $\ddot{X}$ is the structure acceleration.

The damping term in the equation is determined from the energy dissipation in the system. In addition to the usual structural damping, C, experiment and theory both show that the fluid also contributes some damping to the system. For the Laplace regime this comes mainly from the energy dissipated by the structure producing surface waves, although some damping from skin friction will also be present. Assuming that this added damping is proportional to the structure velocity, the total damping term is then:

$$(C + C_a)\ddot{X} \qquad (2.7)$$

where C_a is the added damping from the fluid.

Since in our experiments it was difficult to measure only the damping which was due to the fluid, the total damping of the system was measured and a total damping value, $\lambda = C + C_a$, is used. The structural damping was determined by tests in air and subtracted from the total damping to obtain the added damping values used as a comparison to the theoretical values.

Now, including the stiffness term, K, and a forcing function term, F(t), the equation of motion for a single degree of freedom system in water is:

$$(m + m_a)\ddot{X} + \lambda\dot{X} + KX = F(t) \qquad (2.8)$$

It has been shown [20,26] (see section 5) that m_a and C_a are dependent on the fluid density, the size and shape of the structure and the frequency of oscillation of the body. The dynamic analysis of fluid-structure systems usually involves the determination of the added mass and damping terms and their dependence on the above factors. The present study is concerned with such an evaluation.

5. DIMENSIONAL ANALYSIS OF HYDRODYNAMIC FORCE

As was stated in section 4, for the case of structures in the Laplace regime, the added mass and damping are dependent on the fluid, body size and shape, and the frequency of excitation. The added mass and damping are derived from the hydrodynamic force and it can be shown by a dimensional analysis that these quantities are dependent on the above factors.

In general, for any type of rigid body fluid-structure problem, the fluid force can be given as [26]:

$$\frac{F}{\rho g d D^2} = f\left(\frac{d}{L}, \frac{H}{L}, \frac{D}{L}, Re \right) \tag{2.9}$$

where,

F = fluid force
ρ = fluid density
g = gravitational acceleration
H = wave height
D = structure cross-section (diameter)
d = water depth
L = wave length; for the earthquake problem this represents excitation frequency
Re = Reynolds number = VD/ν where ν is kinematic viscosity and V is velocity

Using the fluid assumptions discussed in section 2.2 for this regime of problem, the dimensionless parameters Re and H/L disappear, as viscous effects are assumed negligible and the wave height is assumed sufficiently small for linear wave theory to apply. The dimensional equation for the hydrodynamic force then becomes:

$$\frac{F}{\rho g d D^2} = f\left(\frac{d}{L}, \frac{D}{L} \right) \tag{2.10}$$

It is seen here that the fluid force is dependent on the fluid density, structure size and frequency of excitation. A similar analysis was carried out by McConnell and Young [29], who came to the same conclusion.

6. DESCRIPTION OF AXIDIF COMPUTER PROGRAM

AXIDIF is the name of a computer program developed at the University of British Columbia for studying fluid forces on offshore structures. The theory and method used in the program to solve such problems are taken from references 26 and 18. It calculates theoretical values of added mass and damping for rigid body, axisymmetric structures in the Laplace regime as a function of excitation frequency.

AXIDIF was developed for the purpose of determining wave loading on structures, but the added mass and damping values derived from it are valid also in the case of the base motion problem, as discussed in Appendix A.

AXIDIF solves Laplace's equation using wave diffraction theory. The velocity potentials for the incoming and reflected wave trains and for the radiated waves due to the structure motions are determined separately and then combined for the total velocity potential. The approach used is based on a boundary element method involving an axisymmetric Green's function [26,18]. The full kinematic and dynamic free surface boundary conditions are incorporated in this way and thus the dependence of the added mass and damping on excitation frequency is included.

The goal of this study is to verify experimentally the added mass and damping values determined from AXIDIF. Once this has been done the program can then be used with confidence to provide these values for the design of full scale structures falling in the Laplace regime.

7. DERIVATION OF ADDED MASS AND DAMPING FROM EXPERIMENT

As will be discussed in later sections, sinusoidal and random tests were used in the experimental program. The sinusoidal tests were conducted over a range of frequencies lying between 0.5 and 6.0 Hz in order to determine the added mass and damping coefficients as a function of excitation frequency. In each frequency test, the forces acting on the test cylinder were determined by measuring its base shear resulting from a known sinusoidal input acceleration. The base shear V(t), for an acceleration excitation a(t), given by:

$$a(t) = \bar{a}\cos(wt) \tag{2.11}$$

where $\bar{a}$ is acceleration amplitude and w is the excitation frequency is:

$$V(t) = \bar{V}\cos(wt + \phi) \tag{2.12}$$

where $\bar{V}$ is the base shear amplitude, and ϕ is the phase shift between the acceleration and base shear records.

A free body diagram of the forces acting on the cylinder is shown in Figure 3. Here, $F_f(t)$ is the fluid force on the cylinder, ma(t) is the inertia force of the cylinder with m being the dry mass of the cylinder, V(t) is the base shear and M(t) the base moment acting on the cylinder at any time t.

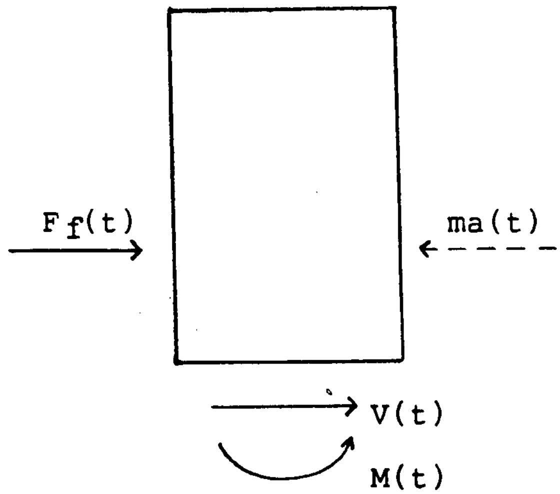

Figure 3 - Free Body Diagram of Forces Acting on Model Cylinder

For a given sinusoidal displacement:

$$X(t) = \bar{X}\cos(wt) \tag{2.13a}$$

where $\bar{X}$ is the amplitude of displacement, the velocity is:

$$\dot{X}(t) = -\bar{X}w\sin(wt) \tag{2.13b}$$

and the acceleration is:

$$a(t) = \ddot{X}(t) = -w^2\bar{X}\cos(wt) \tag{2.13c}$$

where $w^2\bar{X}$ represents the acceleration amplitude $\bar{a}$, previously defined.

Taking equilibrium of forces on the free body diagram (Figure 3), the resulting equation is:

$$F_f(t) + V(t) = ma(t) \qquad (2.14)$$

and applying equations 2.12 and 2.13c to 2.14 gives:

$$F_f + \bar{V}\cos(wt + \phi) = -mw^2\bar{X}\cos(wt) \qquad (2.15)$$

The moment on the cylinder was not considered in this analysis. The base shear can be resolved into its components:

$$V(t) = \bar{V}\cos(wt + \phi) = \bar{V}_1\cos(wt) + \bar{V}_2\sin(wt) \qquad (2.16)$$

where $\bar{V}_1 = \bar{V}\cos\phi$ and $\bar{V}_2 = \bar{V}\sin\phi$. Introducing this into equation 2.15 gives:

$$-mw^2\bar{X}\cos(wt) = \bar{V}_1\cos(wt) + \bar{V}_2\sin(wt) + F_f \qquad (2.17)$$

For sinusoidal input, the fluid force F_f is sinusoidal and can be resolved to represent added mass and added damping as follows:

$$\begin{tikzcd}[column sep=small]
& \text{Sinusoidal Fluid Force} \arrow[dl] \arrow[dr] & \\
\text{Kinetic Energy} \arrow[d] & & \text{Energy Dissipation} \arrow[d] \\
\text{Inertia Force} \arrow[d] & & \text{Damping Force} \arrow[d] \\
\text{In Phase With Motion} \arrow[d] & & \text{In Quadrature With Motion} \arrow[d] \\
\text{Added Mass} = m_a & & \text{Added Damping} = C_a
\end{tikzcd}$$

The fluid force can then be represented as:

$$F_f = F_1\cos(wt) + F_2\sin(wt) = m\ddot{X} + \lambda\dot{X} \tag{2.18}$$

Applying equation 2.18 along with 2.13, equation 2.17 becomes:

$$-mw^2\bar{X}\cos(wt) = \bar{V}_1\cos(wt)+\bar{V}_2\sin(wt)+m_a w^2\bar{X}\cos(wt)+\lambda w\bar{X}\sin(wt) \tag{2.19}$$

Re-arranging 2.19 yields the equation of motion for this problem, similar to equation 2.8, only lacking the stiffness term KX, since the cylinder is rigid:

$$-(m + m_a)w^2\bar{X}\cos(wt) - \lambda w\bar{X}\sin(wt) = \bar{V}_1\cos(wt) + \bar{V}_2\sin(wt) \tag{2.20}$$

On solving for the added mass m_a, and the total damping λ, which includes both structural and fluid damping, one obtains:

$$-(m + m_a)w^2\bar{X} = \bar{V}_1 \quad \text{or} \quad m_a = \frac{-\bar{V}_1}{w^2\bar{X}} - m = \frac{\bar{V}_1}{\bar{a}} - m \tag{2.21}$$

and

$$-\lambda w\bar{X} = \bar{V}_2 \quad \text{or} \quad \lambda = \frac{-\bar{V}_2}{w\bar{X}} \quad \lambda = \frac{\bar{V}_2 w}{\bar{a}} \tag{2.22}$$

The same tests were first performed in air to determine the 'dry' mass and damping values.

It should be noted here that m_a and λ are functions of both excitation frequency w, and displacement $\bar{X}$. By invoking the fluid assumptions of section 2, the problem satisfies the Laplace regime so that the displacement is eliminated as an influencing variable. This fact was checked in this study experimentally by varying $\bar{X}$ at a constant frequency w, and determining m_a and λ for our model.

The experiments were performed to verify the added mass and damping values derived from the Laplace equation. It is important, therefore, that any forces which arise as a result of viscous action do not have a large influence on the added mass and damping values derived from our model tests. Since we are dealing with a real fluid which does have viscosity, it was expected that the measured added mass and damping values would have some dependence on displacement. This condition was, in fact, observed. The effect was small, however, and the experiments therefore represented the characteristics of potential flow reasonably well.

8. DEVELOPMENT OF TRANSFER FUNCTION

The transfer function relating cylinder base shear V in water, with input acceleration a, is a useful design parameter. The transfer function for the rigid cylinder model of this experiment or for any rigid submerged structure can be derived as follows.

The equation of motion for this case, from equations 2.14 and 2.18, can be written:

$$(m + m_a)\ddot{X} + \lambda\dot{X} = V \qquad (2.23)$$

Letting $X = \bar{X}\exp(iwt)$ and $V = \bar{V}\exp(iwt)$, where $\bar{X}$ and $\bar{V}$ are both amplitudes, we get:

$$(m + m_a)(iw)^2\bar{X}\exp(iwt) + \lambda(iw)\bar{X}\exp(iwt) = \bar{V}\exp(iwt) \qquad (2.24)$$

which gives:

$$[\ -(m + m_a)w^2 + \lambda iw\ ]\bar{X} = \bar{V} \qquad (2.25)$$

The transfer function relating base shear to displacement is then:

$$\left|\frac{\bar{V}}{\bar{X}}\right| = \sqrt{(m + m_a)w^4 + \lambda^2 w^2} \qquad (2.26)$$

Using $\bar{a} = w^2\bar{X}$, the transfer function relating base shear to acceleration is:

$$|H(w)| = \left|\frac{\bar{V}}{\bar{a}}\right| = \frac{1}{w}\sqrt{(m + m_a)^2 w^2 + \lambda^2} \qquad (2.27)$$

where m_a and λ are functions of frequency w, as stated earlier in section 5. These values can be derived from experiment or theory.

9. DERIVATION OF TRANSFER FUNCTION FROM EXPERIMENTS

As stated in section 7, this study involved sinusoidal and random testing. The sinusoidal tests were used to determine added mass and damping values as a function of frequency, which were compared to the theoretically derived values. They were also used to develop the transfer function by taking the ratio of the input to the output at each frequency value (equation 2.28).

$$H(w) = \frac{V(w)}{a(w)} \qquad (2.28)$$

The random tests were used also to develop, experimentally, the transfer function relating base shear to input base acceleration for the cylinder model. This latter transfer function was then used to check the validity of the transfer function derived theoretically. The added mass and damping values of the theoretically determined transfer function were derived using the AXIDIF computer program.

In the random tests, earthquake excitations a(t), were used to excite the cylinder in water. The random base shear V(t), was recorded. The power spectral densities, Sa(w) and Sv(w) corresponding to a(t) and V(t) respectively, were calculated from:

$$Sv(w) = \left[\int_{-\infty}^{\infty} V(t)e^{-iwt}dt\right]^2 \tag{2.29}$$

and

$$Sa(w) = \left[\int_{-\infty}^{\infty} a(t)e^{-iwt}dt\right]^2 \tag{2.30}$$

These power spectral densities were evaluated using a Fast Fourier Transform (FFT) computer program. From random analysis theory [2,7], the transfer function is then calculated as:

$$|H(w)|^2 = \frac{Sv(w)}{Sa(w)} \tag{2.31}$$

The measured output base shear spectrum, Sv(w), was also compared to the spectrum derived theoretically. This was accomplished by multiplying the input base acceleration spectrum of the earthquake record by the theoretically derived transfer function. The experimental base shear spectrum was determined by performing a Fourier analysis of the recorded output data.

III. MODEL AND TESTING APPARATUS

It was the intention in this study to create experiments which represented a structure undergoing base motion in the Laplace regime of fluid-structure interaction. The conditions necessary to qualify for this regime were outlined in chapter two. As described in the following sections, a model and testing apparatus were developed which enabled these conditions to be satisfied.

1. DEVELOPMENT OF TESTING APPARATUS

The testing was performed in the Seismic Simulation Laboratory of the Civil Engineering Department at U.B.C. This laboratory contains a single degree-of-freedom shaking table capable of a maximum peak-to-peak displacement of six inches. A PDP-11 mini-computer is used to operate the table. It is capable of exciting the table with sinusoidal frequencies from 0.0 to 30.0 Hz and with simulated earthquake records which are stored on tape. The table was used to produce the sinusoidal and random base excitations on the model. The PDP-11 was also used to tabulate and process all of the data recorded in the experiments. Figure 4 shows a photograph of the shaking table.

A water tank was constructed to straddle the table so that the model could be set into motion underwater. The goal in designing the tank was to create the required fluid conditions for testing and to enable the model to be properly excited through the base by the table. The required fluid conditions were:

i) no wave reflection from the walls.

ii) no water disturbances caused by the table motion other than through the test model.

iii) no viscous interaction between the tank walls and the model.

In addition to these requirements, it was also desired to construct a facility which could incorporate future testing of a variety of models and experiments.

Two similar studies involving experimental tests [4,6], used a water tank with the shaking table acting as the floor of the tank. It was felt that this approach would not be suitable in the present test case since the U.B.C. table moves by rocking on four legs and thus has a small vertical component which would cause water disturbances. It was decided to construct the tank independent of the table with only the model base in contact with the moving table. As a result, the table was designed to completely straddle the table and to be supported on the laboratory floor surrounding it. A hole was cut in the center of the tank floor, through which the model could be fastened to the table. Figure 5 is a photograph of the tank and model apparatus.

Figure 6 shows a schematic of the tank. The tank dimensions are 12 X 13 X 4 feet and it consists of a steel frame with plywood sheathing. A plastic pool liner is used as a seal. Horse hair filters are placed around the inside perimeter of the tank to dissipate the surface water waves and prevent them from being reflected back from the walls. The tank is supported by ten legs around its perimeter, which rest on the floor surrounding the table.

Since the model was attached to the shaking table through a hole in the tank floor, it was necessary to design a watertight seal at the assembly base to allow for the motion of the model. Figure 7 shows the sealing arrangement used. An aluminum plate was fastened to a rigid wood block which was mounted to the table through a plywood sheet. The model base was attached to this plate. Another aluminum plate was sealed into the bottom of the tank at its center through which an 18 inch hole was placed. A round rubber sheet was then fastened between the base plate on the table and the plate on the bottom of the tank by means of a stainless steel sealing ring. This formed a seal between the tank and the table allowing full transfer of table motion to the model. To prevent fluid disturbances from this mounting apparatus, an aluminum sealing ring, which reduced the hole diameter to 9 inches, was used to seal the rubber to the tank floor. Over this aluminum ring, a smaller 14 inch diameter plexiglass disc was attached to the model support. This effectively kept the water set into motion by the mounting apparatus from disturbing the water surrounding the model.

Figure 4 - Photograph of Shaking Table

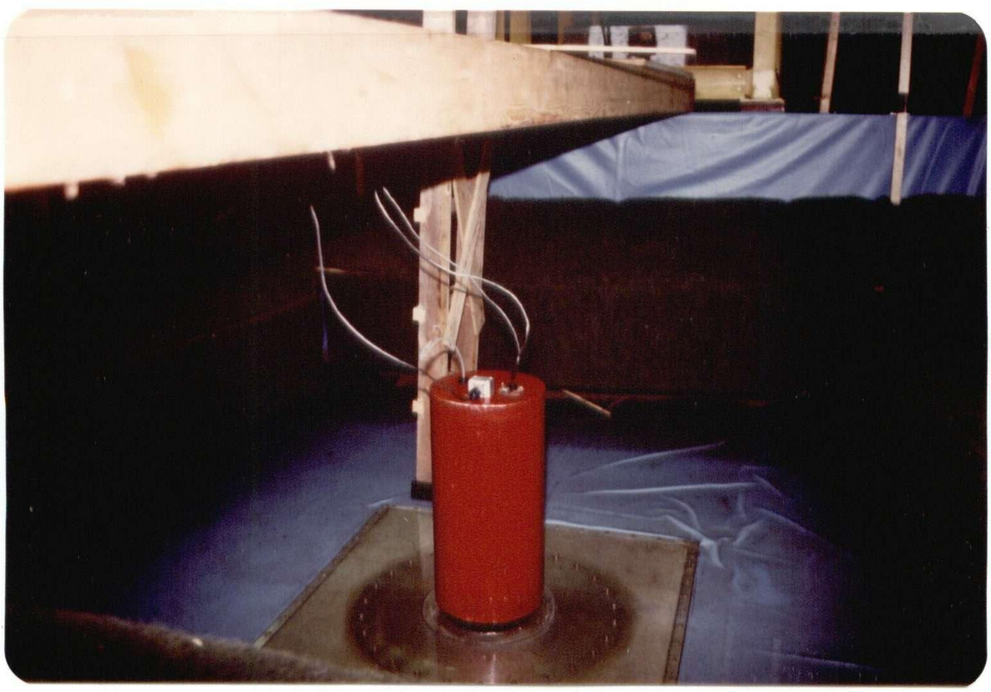

Figure 5 - Photograph of Tank and Model Apparatus

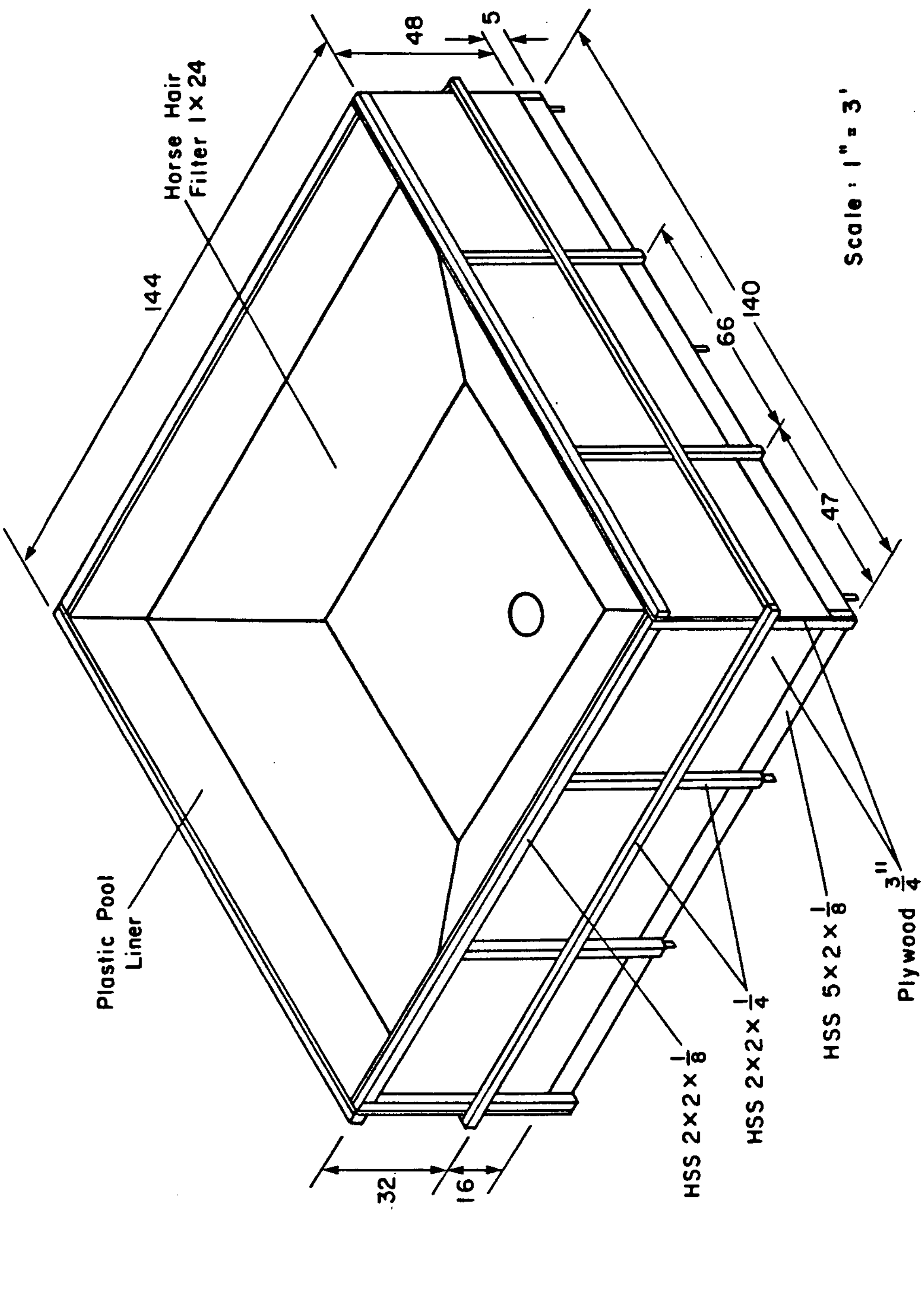

Figure 6 - Schematic of Testing Tank

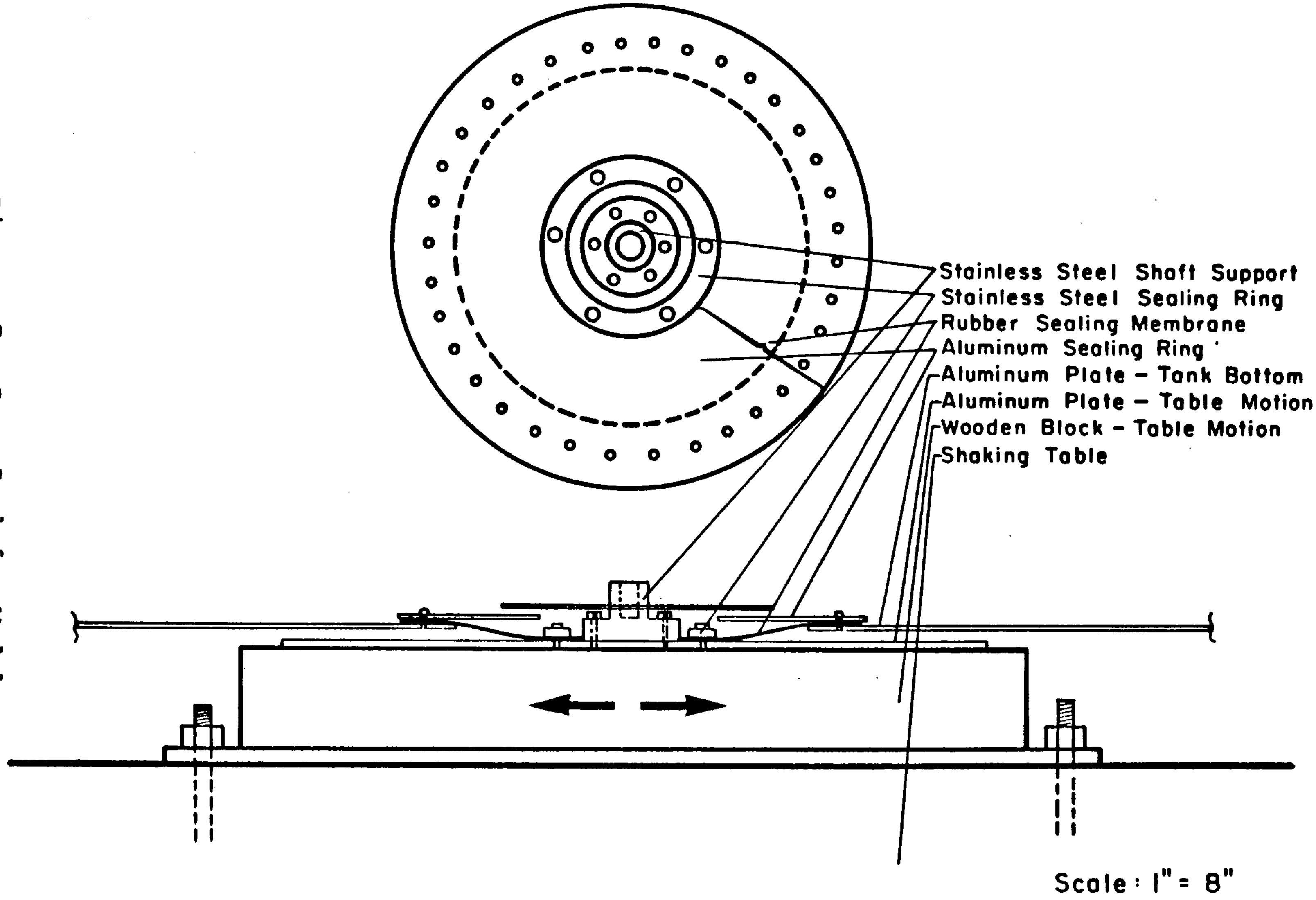

Figure 7 - Base Seal for Model

2. DESIGN OF MODEL

The test model was selected to satisfy the requirements for a potential flow situation. The available AXIDIF computer program yields a theoretical solution to Laplace's equation for axisymmetric bodies. Accordingly, a cylindrical model was chosen for the tests, since this is the simplest shape for representing the Laplace regime and, as well, it is quite common in offshore construction. Furthermore, the few existing experimental studies which are available for comparison purposes also used cylindrical shapes.

The dimensions of the cylinder were chosen so as to meet the requirements of no flow separation (Keulegan-Carpenter Number < 2). This corresponds to a maximum allowable displacement to diameter ratio of $A/D < 1/\pi$ or $D/A > \pi$ (see chapter 2). The maximum base amplitude used in the tests was 1.5 inches. An 11 inch diameter cylinder was chosen, such that $D/A = 11/1.5 = 7.3 > \pi$.

The cylinder model is shown in Figure 8. It is 22 inches high and made of aluminum. The cylindrical shell itself is meant to be rigid. It consists of a 3/32 inch outer shell with a 3/4 inch plate at the top and a 1/8 inch plate on the bottom. The cylinder is attached rigidly to the top of a 1 and 1/4 inch diameter steel shaft which is fastened at the bottom to the shaking table through a stainless steel base. The cylinder is made water tight by sealing the 4 inch diameter hole through which the shaft passes in its bottom with a rubber membrane. The result of this arrangement is that all force on the outside of the cylinder is transferred to the top of the shaft. The shaft then acts as an end loaded cantilever through which we can measure the total force on the cylinder.

The criteria for designing the model were:

i) to have it act as a rigid cylinder

ii) to have the steel shaft flexible enough to measure strains at all load levels

iii) to have the natural frequency of the system high enough so as not to cause any resonant interference with the test frequencies used (preferably above 20 HZ).

Meeting these criteria proved to be quite difficult. It was not possible to select a steel shaft which was flexible enough to measure small strains yet stiff enough to have a natural frequency above 20 Hz. The design finally settled on had a natural frequency in water of about 16 Hz (determined from free vibration tests); the small strains developed were measured with the aid of considerable electronic amplification.

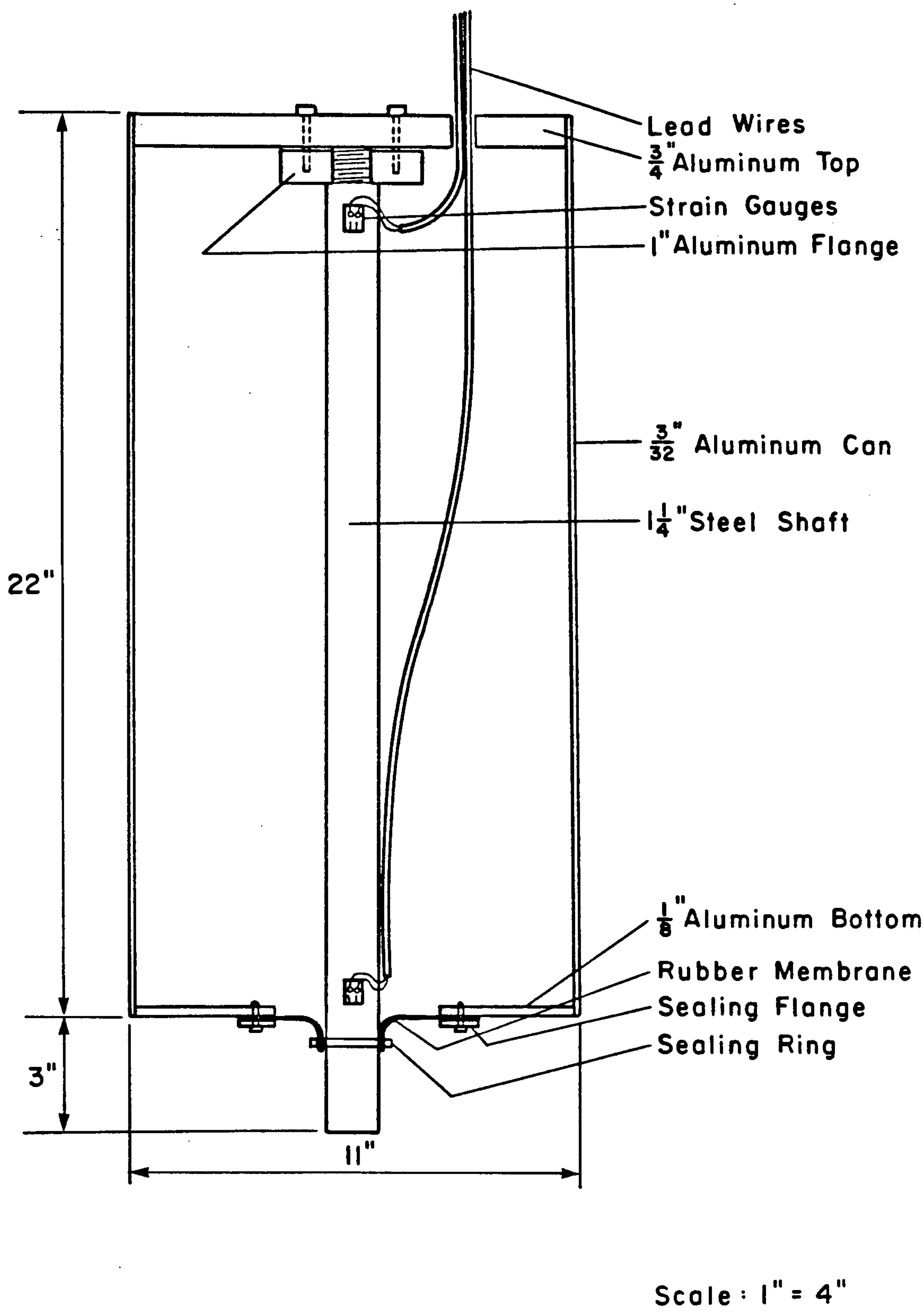

Figure 8 - Diagram of Model Cylinder

3. DATA MEASUREMENT

As discussed in chapter 2, the data necessary for determining the added mass and damping values in these tests was the input base acceleration record, a, and the resulting cylinder base shear record, V. In addition to these values, the displacement of the base, X, also was measured to keep track of its value during the tests and as a check on the acceleration record through the simple harmonic relation $a=-w^2X$, where w is the harmonic input frequency.

The displacement was measured by means of an LVDT situated on the shaking table. The acceleration was recorded by an accelerometer attached to the table. This latter record was used in analysis instead of the known excitation record in order to account for any discrepencies between the input command motion and the actual recorded table motion.

The base shear was measured by a Wheatstone bridge arrangement using four strain gauges mounted on the steel shaft. The steel shaft, base and strain gauges are shown in the photograph of Figure 9. This system measured the strains at the top and bottom of the shaft, from which the moments at these points could be calculated. Thus

$$M = \frac{\epsilon EI}{y} \tag{3.1}$$

where

M = moment

ϵ = strain measured

E = Young's modulus of the shaft material

I = moment of inertia of the shaft cross section

y = distance between the neutral axis and the surface of the shaft

The Wheatstone bridge set up also yielded the difference between the top and bottom moments, after which the base shear could be determined from:

$$V_{base} = \frac{M_{top} - M_{base}}{\text{height of shaft}} \tag{3.2}$$

The model was calibrated initially through static load tests which correlated a given base shear value with a voltage output from the bridge. The calibration curve was linear.

The required data from the tests were the amplitudes of the base shear, V, the base acceleration, a, and the phase shift between these variables, ϕ. More information on how the data were recorded and processed to give the above values is provided in Appendix B.

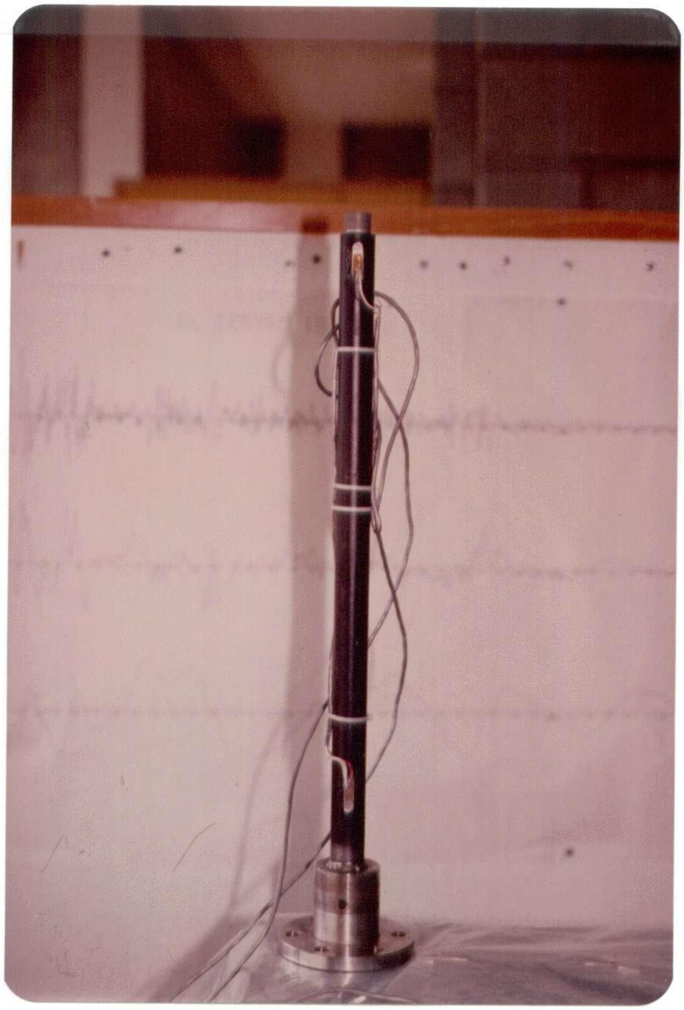

Figure 9 - Photograph of Steel Shaft, Base and Strain Gauges

IV. DESCRIPTION OF EXPERIMENTS

The purpose of this study was to experimentally determine the dynamic characteristics of submerged structures due to seismic loading. The dynamic characteristics of interest are the added mass and damping due to the fluid. The theoretical derivation of the frequency transfer function, H(w), relating base shear to base acceleration was also tested experimentally. Of particular interest in this study is the frequency dependence of the added mass and damping values, which is significant at the lower end of the frequency scale and in surface piercing structures which produce surface waves. The testing consisted of two phases:

1) Sinusoidal tests between 0.5 and 6.0 Hz which is the frequency range of importance in most recorded earthquakes.

2) Random motion tests, using records of actual earthquakes, to confirm the theoretically derived transfer function between input base acceleration and output base shear on the cylinder

The tests were carried out with the cylinder in two situations:

1) Surface Piercing

2) Submerged to a depth of one times the cylinder radius

1. SINUSOIDAL TESTS

The first set of sinusoidal tests were done at frequency levels of 0.5, 1.0, 1.5, 2.0, 2.5, 3.0, 4.0, 5.0, and 6.0 Hz. After these were analyzed it was realized that the greatest fluctuation in added mass and damping values occurred below 2.5 Hz, so additional testing at increments of 0.25 Hz was conducted in this range. Photographs of the sinusoidal testing being performed are shown in Figures 10 and 11.

The analysis for added mass and damping was based on linear wave theory (chapter 2). This was checked visually in the testing and controlled by reducing the input amplitude if any peaking or nonlinear wave characteristics appeared. At the lower frequencies this was not a problem and quite large amplitudes could be used. However, at the higher frequencies the amplitudes had to be kept small in order to prevent the waves from breaking and becoming nonlinear. This situation would probably be reflected in real earthquake loading, as displacements at higher frequencies are usually not large.

In applying Laplace's equation, it is necessary that the added mass and damping values be independent of displacement, which means that viscous effects are considered to be negligible. In reality, of course, water is viscous and some effects on the results are to be expected. This was checked by running tests at a given frequency for several displacement amplitudes and determining added mass and damping values. The results of this study are shown in Figures 12 and 14, where more than one value of added mass and damping is noted at a given frequency.

When the results were first analyzed, it was suspected that at higher frequencies there was some amplification in the acceleration of the top of the cylinder relative to the base value, presumably as a result of approaching a resonant condition for the model. This would result in the cylinder undergoing a rocking mode rather than a pure translational mode. This was checked by repeating the tests with an accelerometer attached to the top of the cylinder as well as to the bottom. A small increase in the top acceleration was noted at higher frequencies and could be accounted for through the resonant amplification factor:

$$a_{top} = a_{base}\left[\frac{1}{1 - \left(\frac{w}{w_n}\right)^2}\right] \tag{4.1}$$

where w is the excitation frequency and w_n is the natural frequency of the model in water (16 Hz). A correction was applied to account for this small effect when analyzing the data, as discussed in the next chapter.

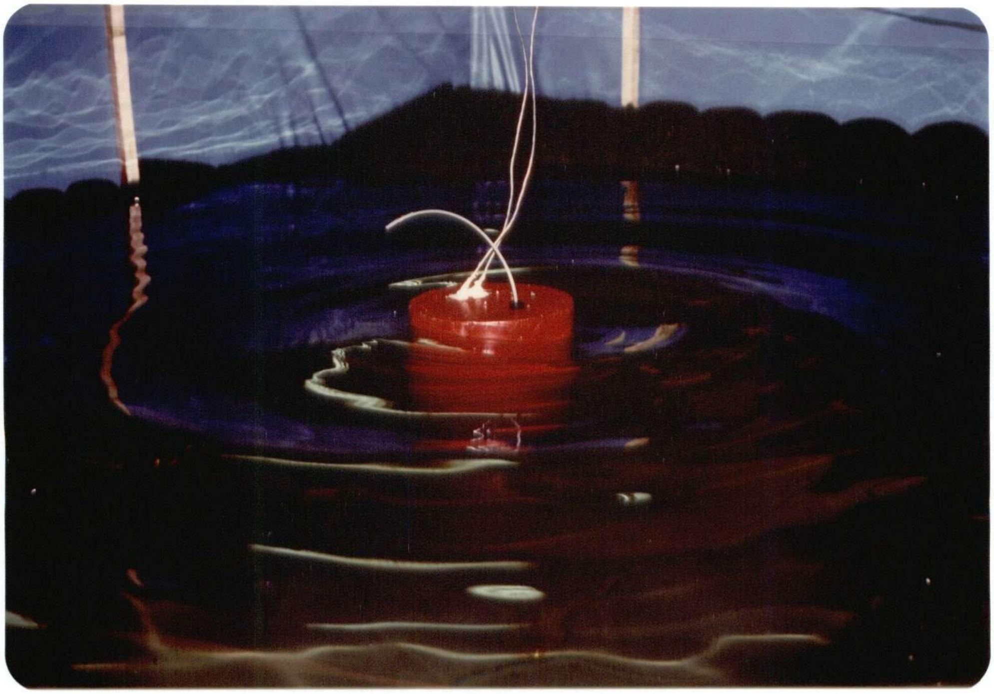

Figure 10 - Photograph of Sinusoidal Test

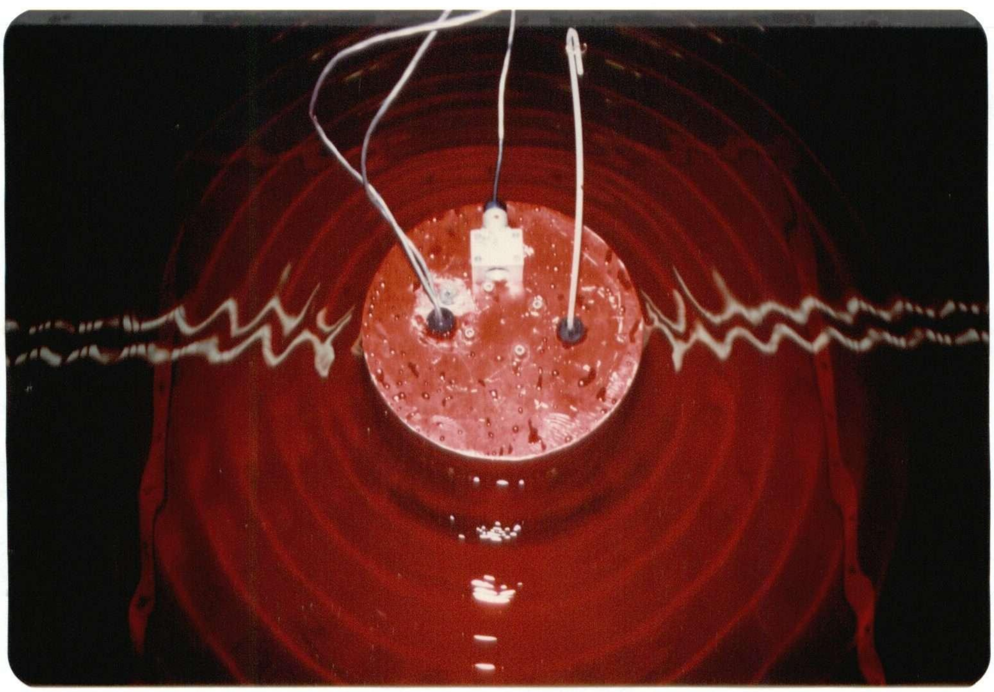

Figure 11 - Photograph of Sinusoidal Test

2. RANDOM TESTS

As was shown in chapter 2, the transfer function for the model can be determined experimentally from random testing. The transfer function can also be evaluated experimentally from a series of sinusoidal tests. The former approach serves as a verification of the theoretical transfer function in pseudo earthquake loading. The base acceleration, a(t), and base shear, V(t), time histories were recorded for input excitations of the El Centro N-S, 1940 and San Fernando S74W, 1971 earthquakes. The earthquake data were taken from taped records of the actual earthquakes.

In order to keep the displacements within the limits of the shaking table and of the model during testing, the earthquake records were scaled in amplitude to an acceptable level. Again the wave condition was monitored visually; no nonlinear characteristics were observed.

The time series data were transferred into the frequency domain in the form of power spectral density functions by way of a Fast Fourier Transform program. These power spectral density functions were then employed to calculate an experimental transfer function, which was used to check the theoretical values. Also, the spectral density of the output derived using the theoretical transfer function was compared to the spectral density of the recorded output data. The time series derived from this theoretical spectral density of the base shear output was also compared to the time series output recorded during the random test.

3. SURFACE PIERCING AND SUBMERGED TESTS

The frequency dependence of the added mass and damping values results from energy dissipation in the system due to the production of surface waves. Byrd [4] and Liaw and Chopra [19], discussed this effect. This frequency dependence is accounted for in the analytical determination by incorporating full dynamic and kinematic free surface boundary conditions in the solution of Laplace's equation.

Frequency dependence is most significant for surface piercing structures at low freqencies. As the structure is submerged, and as the frequency increases, it has less tendency to produce surface waves, and the frequency dependence becomes negligible. Liaw and Chopra show this theoretically in solving Laplace's equation for potential flow and Byrd shows this experimentally in his tests on models which are submerged and are excited at higher frequencies.

Byrd defined a factor, $2\pi g/w^2$, which is the wavelength for a wave of frequency w, such that if the depth of submergence of the structure is greater than this value, the effect of surface waves diminishes. This factor also gives an indication of the effect of frequency on the hydrodynamic force. For lower values of frequency, the factor is large, indicating higher frequency dependence and this reduces quickly for increasing frequency values.

In order to explore this condition, tests were performed on both a surface piercing cylinder and a cylinder submerged to a depth of one times its radius under the surface. It was expected, and indeed observed, that the frequency dependence of the added mass and damping for the surface piercing cylinder was much more significant than for the submerged case. The frequency values tested (0.5 - 6.0 Hz) were also in the frequency range necessary to investigate this dependence. Byrd's tests were carried out above 3 Hz. Earthquakes can be expected to contain considerable power below this frequency so that an investigation below this 3 Hz limit was considered to be desirable.

V. RESULTS AND DISCUSSION

1. ADDED MASS FOR SURFACE PIERCING CYLINDER

The added mass values were determined as a function of frequency through a series of sinusoidal tests as discussed in chapter 4. The base acceleration and base shear time history records were processed as discussed in appendix B to obtain the peak values and phase shifts. These values were then used as shown in chapter 2 to calculate the added mass. The theoretical values of added mass versus frequency were determined using the computer program AXIDIF, which solves Laplace's equation for potential flow (chapter 2 and appendix A).

Figure 12 shows the added mass versus frequency for the surface piercing cylinder. The added mass is plotted as a dimensionless value, $m_a/\rho r^3$, where ρ is water density and r is the radius of the cylinder. The agreement between experiment and theory is very good.

It is important first to note the large fluctuation in the curve below 2.5 Hz. The frequency dependence of the added mass is quite evident at frequencies less than this value. As the frequency increases above 2.5 Hz, the added mass tends to be a constant, independent of frequency. This agrees well with the experimental work of Byrd [4], who carried out tests above 3.0 Hz and obtained a constant value of added mass, independent of frequency. This also agrees well with the theoretical work of Liaw and Chopra [19], whose results for hydrodynamic force were previously shown in Figure 2.

The radiation of surface waves by a moving structure is classified as a dispersive type of energy propagation [2]. This means that the velocity of the energy propagation wave is dependent on the frequency of oscillation of the structure. The propagation velocity increases with the excitation frequency for the case of surface wave production by a moving structure. The phase shift between the velocity of the structure and the velocity of the propagating waves also varies. It is this phase shift that causes the large fluctuation in added mass and damping at the low end of the frequency scale and not at the higher end. This was noted in the experiments, where the phase shift between the structure acceleration (velocity) and the fluid force on the structure exhibited the same peaking tendencies as the added mass and damping curves - starting at 0° for 0. Hz, rising to a peak at about 1.0 Hz and then dropping back to 0° as the frequency increased.

The degree of fluctuation in the added mass values also depends on the depth of the structure. The dependence on frequency is more significant for shallow structures, where a greater percentage of the body surface is affected by wave action. For the surface piercing case it might be expected that the frequency dependence would be most significant for shallow, large diameter structures which have a high percentage of surface area in contact with surface waves. The effect would be least significant for tall, deep, small diameter structures (but still falling within the Laplace regime). This effect is apparent if one uses the AXIDIF program to solve the problem theoretically for various sizes of cylinders.

It should also be noted in Figure 12 that there is more than one value of added mass plotted for most of the frequency values tested. This arises from the dependence of added mass on displacement, which is related to the fact that water is viscous, and not a true ideal inviscid fluid. As discussed in chapters 2 and 4, this was checked by running several sinusoidal tests at different displacement amplitudes for a single frequency value. Of course, this variation does not show up in theory, as the solution of Laplace's equation for potential flow imposes the assumption of inviscid flow. As can be seen, the effect is quite small and it appears that our tests satisfied the requirements of potential flow quite well, and that the viscous effects were negligible.

From Figure 12, it may be concluded that the added mass values can be accurately derived from theory using the AXIDIF program.

2. ADDED MASS FOR SUBMERGED CYLINDER

Tests were also performed on a submerged cylinder and the data were processed in the same manner as for the surface piercing cases. Fewer tests were carried out, since these were primarily intended for comparison with the surface piercing cylinder. Also, since the added mass did not fluctuate significantly with frequency, it was not necessary to have a fine variation in the frequency.

Figure 13 shows the results of these tests. There is good agreement between the experimentally and theoretically derived added mass values. By comparing Figure 13 with Figure 12, it may be concluded that the frequency dependence of the added mass for the submerged case is negligible. This agrees well with the findings of Byrd [4], and Liaw and Chopra [19]. Physically, this can be explained by the fact that the structure is unable to produce any surface waves when it is submerged. This was verified in the tests, during which no apparent surface disturbances of the water were observed.

The values derived theoretically can be used quite satisfactorily in calculating the transfer function for the submerged cylinder. Also, since added mass is essentially frequency independent in this case, a theoretical solution ignoring the free surface kinematic and dynamic boundary conditions should give good values for the added mass of a submerged cylinder. This solution is much easier to obtain, and since it is independent of frequency, only has to be solved once for a given structure.

3. ADDED DAMPING

The added damping, which results from the energy dissipated in producing surface waves, was determined from the sinusoidal data according to the method described in chapter 2. Figures 14 and 15 show the results for the surface piercing cylinder and the submerged cylinder respectively.

The experimental and theoretical values agree quite well. As for the added mass values, the peaks occur at the low end of the frequency range.

Figure 14 shows the influence of displacement amplitude at any one frequency on the added damping. As noted in the added mass results, this is related to the influence of fluid viscosity.

In comparing Figures 14 and 15, it is noted that the damping values for the surface piercing case are much greater than for the submerged case. This is to be expected, since the surface waves diminish as the structure is submerged.

The graphs are plotted in dimensionless values, $C_a/w\rho r^3$, where C_a is the added damping in kg/s, kg is kilograms, s is seconds, w is frequency, ρ is water density and r is the radius of the cylinder. The peak value for the surface piercing cylinder, Figure 14, corresponds to about 3.5% of critical damping for the model. The peak for the submerged case is less than 1.0% of critical damping.

4. TRANSFER FUNCTIONS

Tests using both sinusoidal and earthquake records were used to develop experimental transfer functions as discussed in chapter 2. These experimentally derived transfer functions were then used to check the validity of the theoretical transfer functions determined from the solution of Laplace's equation (see chapter 2.8).

Figures 16 and 17 show the results for the surface piercing and submerged cylinders respectively from the sinusoidal tests. The comparison is quite good in both cases. For the surface piercing cylinder (Figure 16), the peaks from the sinusoidal tests are larger than the corresponding theoretical values.

Figures 18 and 19 show the comparison of the experimental and theoretical transfer functions for the surface piercing cylinder when subjected to the El Centro N-S 1940 and the San Fernando S74W, 1971 earthquakes respectively. Figure 20 shows the comparison between these functions for the submerged case for the El Centro earthquake record.

The surface piercing cylinder transfer function is quite frequency dependent. For input accelerations in the lower frequency range (< 3 Hz), this becomes important. If the solution was obtained ignoring the wave radiation boundary condition, and thus ignoring frequency dependence, the resulting forces from input accelerations below 3 Hz would be unconservative. The analysis would not accurately represent the real situation.

As would be expected, the transfer function for the submerged cylinder does not show as much frequency dependence as the surface piercing case.

Figures 21 and 22 show the spectra of the output base shear for the surface piercing and submerged cylinders respectively. The solid lines indicate the results obtained by multiplying the spectrum of the input acceleration record by the theoretically derived transfer function (equation 2.27). The broken lines are the spectra of the base shear recorded in the random tests. The theoretical transfer functions predict good results.

Comparison between experimental and theoretical results is generally considered to be best performed in the frequency domain for random tests [2]. However, the time series output derived theoretically was also compared to the time series output data of the El Centro test (Figure 23). This was obtained by multiplying the complex frequency spectrum of the input acceleration by the complex transfer function derived from theory and then performing an inverse Fourier transform to obtain the output time series.

The agreement between experiment and theory was quite good in all cases. This establishes the validity of using the theoretical AXIDIF computer program for developing transfer functions for offshore structures.

5. RESONANT EFFECTS IN THE MODEL

The theoretical solution applies to a cylinder undergoing rigid body acceleration in water. As discussed in chapter 3, the model had to be flexible enough to measure the hydrodynamic forces developed, yet stiff enough to act as a rigid body. The natural frequency of the model in water, measured from free vibration tests, was 16 Hz. At the higher frequency range, towards 6 Hz, the cylinder moved in a rocking mode, while the cylinder shape remained rigid, and, as a result, some amplification of the acceleration at the top of the cylinder with respect to the base acceleration was noted. This amplification was small and could be determined by equation 4.1; this fact was checked by measuring the accelerations at the top and base of the cylinder.

To correct for this condition, the acceleration at the center of gravity of the cylinder was determined from:

$$a_{CG} = a_{BASE}\left\{1.0 + 0.64\left[\frac{1}{1 - (\frac{w}{w_n})^2} - 1\right]\right\} \qquad (5.1)$$

and used in the calculations for the added mass and damping. Here, a_{CG} is the acceleration of the center of gravity of the cylinder and 0.64 is the relation of the position of the center of gravity to the height of the cylinder.

6. VISCOUS EFFECTS

The assumption of inviscid fluid is made when applying Laplace's equation for potential flow. The model and experiments were designed to satisfy the requirements of this situation as closely as possible. However, water is viscous and it was anticipated that this condition might influence the experimental results. The viscosity of the water could be expected to cause:

i) the added mass and damping values to exhibit a small dependence on displacement amplitude

ii) some additional damping due to skin friction drag forces

The dependence on displacement amplitude has already been discussed in sections 1 and 3 of this chapter. This effect did show up, but it was quite small and could be neglected in the analysis.

Any viscous damping forces which were present would be included in the added damping measured in the experiments. To verify that this viscous term was quite small in relation to the total damping, the total drag force on the cylinder (which for this case is the drag force from skin friction only) was estimated by employing the approximate expression [26]:

$$F_d = 1/2 C_d A_p l \rho |\dot{u}| \dot{u} \qquad (5.2)$$

where;

F_d= viscous drag force on the cylinder

C_d = drag coefficient, taken equal to 1.0

A_p = projected area of cylinder

ρ = density of water

l = length of the cylinder

$|\dot{u}|$ = absolute value of u

$\dot{u}$ = peak relative velocity between the cylinder and the water

The nonlinear term, $|\dot{u}|\dot{u}$, was linearized using $|\dot{u}|$ = $(\sqrt{8}/\pi)\sigma_{\dot{u}}$ for small amplitudes [26], where $\sigma_{\dot{u}}$= root mean square of the velocity which equals $\dot{u}/\sqrt{2}$ for sinusoidal motion. This viscous drag term was calculated for each of the tests and found to be small in relation to the total damping term which consisted of both the wave radiation and viscous damping terms: it had a maximum value of 9% of the total damping value and was less than 5% for most of the tests. The assumption of inviscid flow therefore seems to be quite reasonable for these tests.

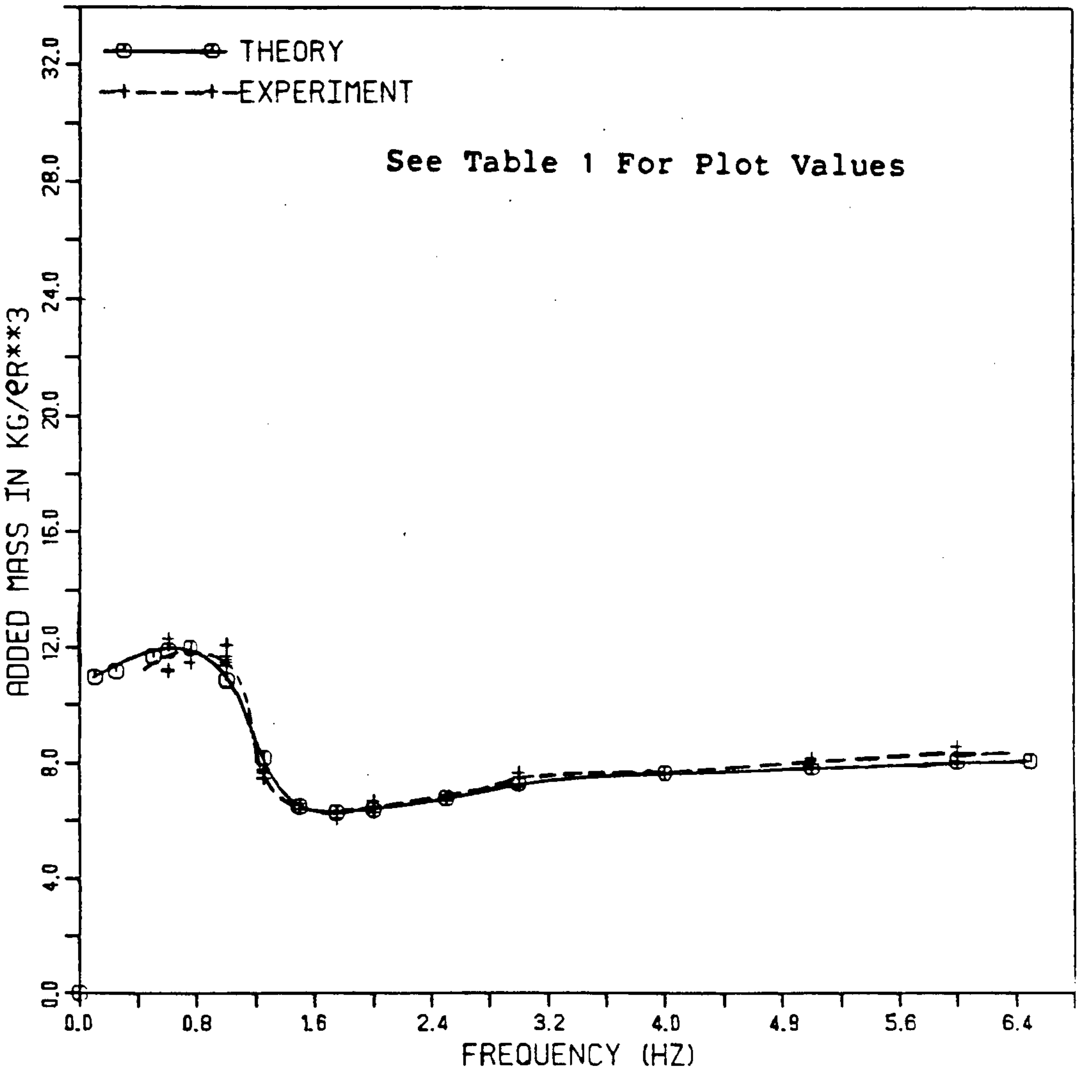

Figure 12 - Added Mass for Surface Piercing Cylinder

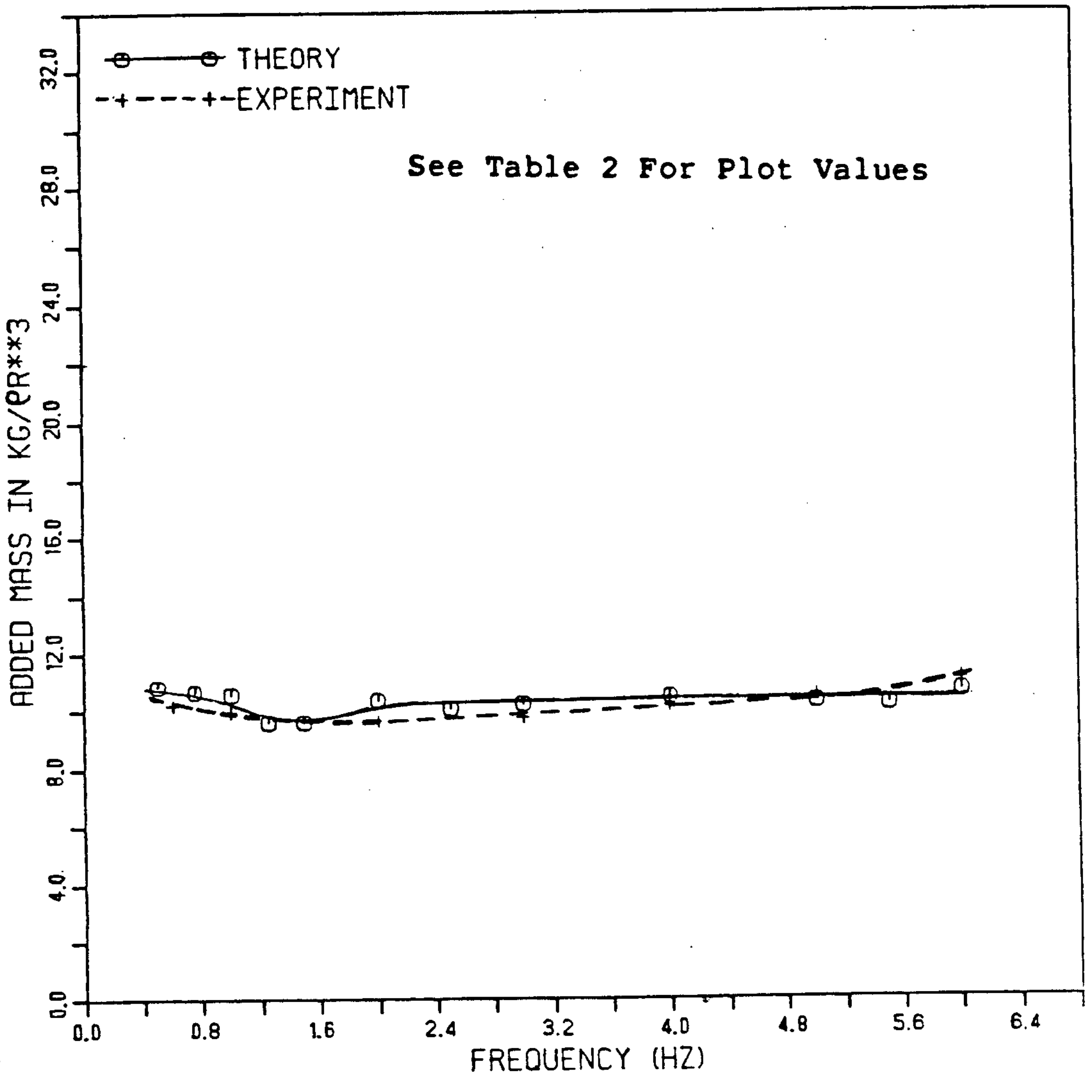

Figure 13 - Added Mass for Submerged Cylinder

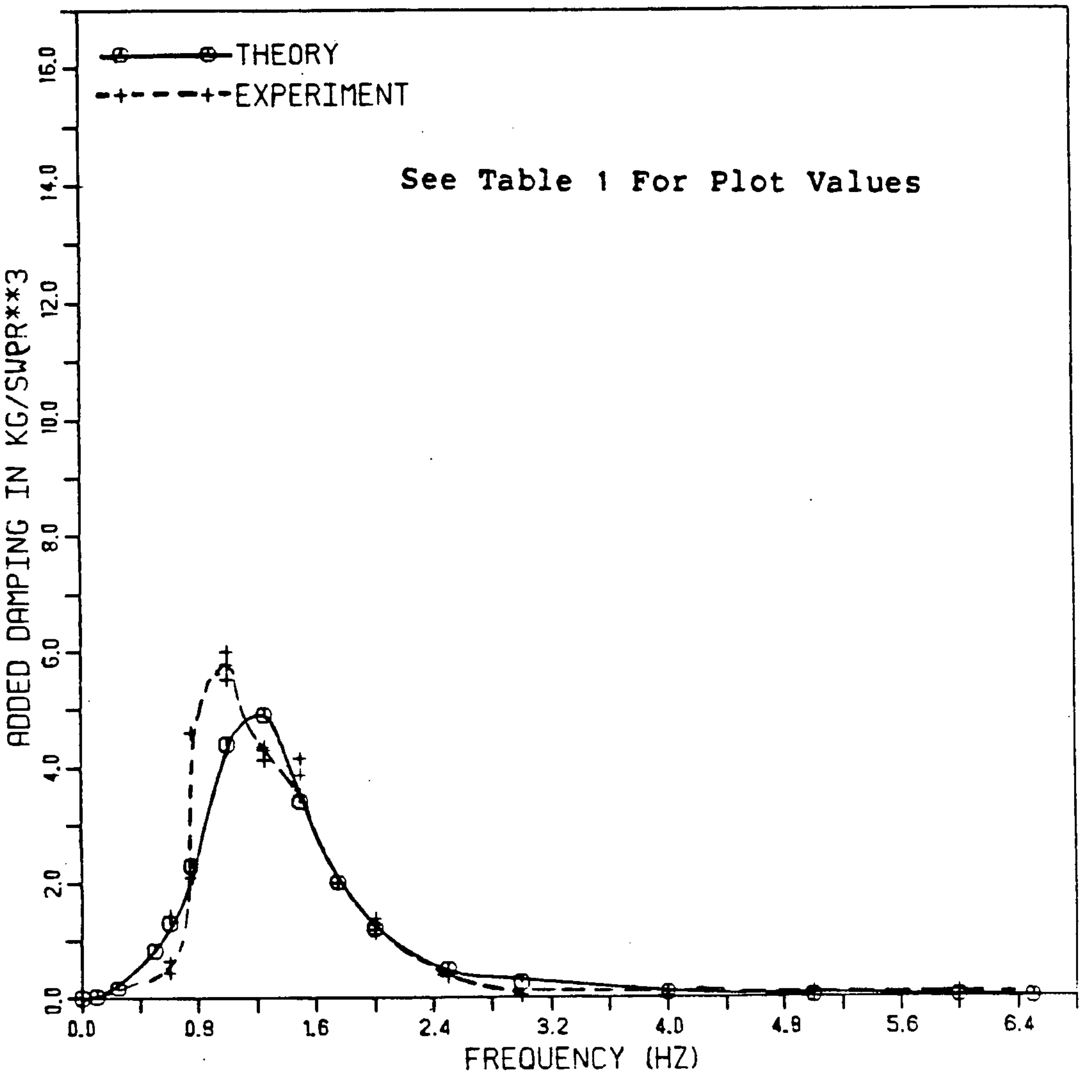

Figure 14 - Added Damping for Surface Piercing Cylinder

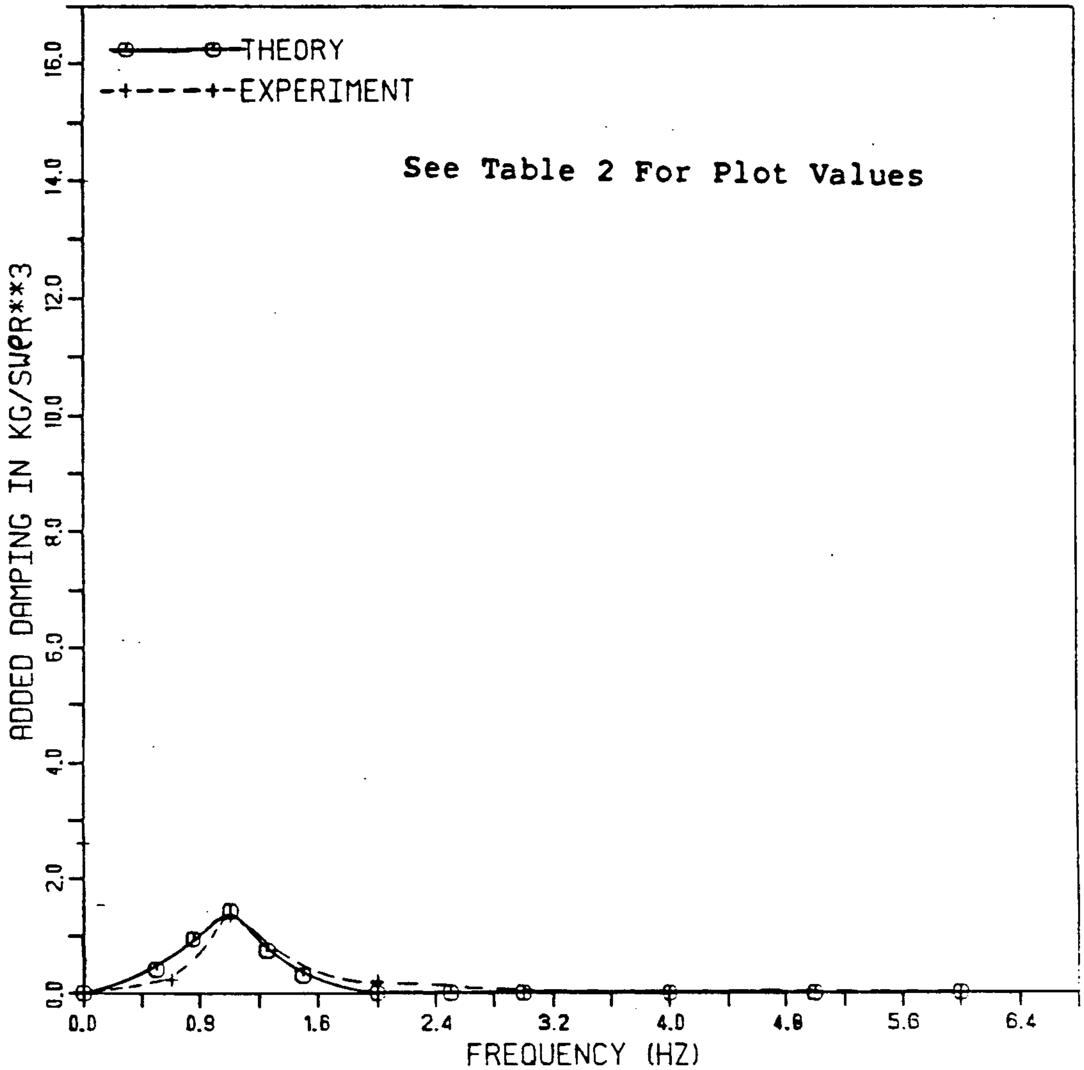

Figure 15 - Added Damping for Submerged Cylinder

Experiment						Theory	
Frequency (Hertz)	Base Shear (N)	Acceleration (m/s^2)	Displacement (cm)	Added Mass ($\frac{kg}{\rho r^3}$)	Added Damping ($\frac{kg}{s w \rho r^3}$)	Added Mass ($\frac{kg}{\rho r^3}$)	Added Damping ($\frac{kg}{s w \rho r^3}$)
0.6	6.61	0.165	1.75	11.2	1.43	11.9	1.3
	13.6	0.314	2.31	12.3	0.63		
	5.5	0.134	1.38	11.24	1.43		
0.75	15.6	0.364	1.75	11.5	2.02	12.0	2.3
1.0	39.8	0.907	2.37	11.4	6.0	10.9	4.4
	22.7	0.513	1.30	11.6	5.5		
	10.8	0.236	0.614	12.1	5.8		
	19.6	0.413	1.09	11.7	6.7		
	26.9	0.587	1.54	11.5	6.6		
1.25	20.7	0.633	1.05	7.7	4.12	8.2	4.9
	20.9	0.643	1.08	7.5	4.36		
	14.3	0.431	0.723	7.8	4.31		
1.5	17.2	0.577	0.69	6.6	4.14	6.5	3.4
	15.1	0.527	0.606	6.4	3.5		
	20.0	0.673	0.782	6.6	3.9		
1.75	39.6	1.48	1.24	6.1	2.0	6.3	2.0
2.0	17.5	0.641	0.416	6.5	1.2	6.4	1.2
	35.4	1.32	0.859	6.3	1.4		
	10.6	0.391	0.26	6.3	1.1		
	50.5	1.81	1.21	6.7	1.5		
	28.2	1.02	0.665	6.5	1.3		
2.5	50.7	1.83	0.74	6.7	0.35	6.8	0.5
3.0	40.6	1.39	0.402	7.3	0.03	7.3	0.25
	81.6	2.8	0.80	7.2	0.01		
	22.8	0.74	0.22	7.7	0.07		
4.0	35.8	1.17	0.181	7.64	0.0	7.7	0.08
	53.8	1.75	0.27	7.65	0.08		
	59.7	1.96	0.30	7.7	0.03		
5.0	77.1	2.43	0.23	8.2	0.12	7.9	0.04
	80.9	2.61	0.236	7.9	0.0		
	76.0	2.4	0.209	8.0	0.0		
	40.3	1.27	0.120	8.2	0.0		
6.0	54.8	1.65	0.105	8.6	0.0	8.1	0.03
	54.5	1.7	0.106	8.1	0.1		

N=Newtons m=meters s=seconds cm=centimeters kg=kilograms
ρ=density r=radius w=frequency

Table I - Recorded Data - Surface Piercing Cylinder

Experiment						Theory	
Frequency (Hertz)	Base Shear (N)	Acceleration (m/s^2)	Displacement (cm)	Added Mass ($\frac{kg}{\rho r^3}$)	Added Damping ($\frac{kg}{s w \rho r^3}$)	Added Mass ($\frac{kg}{\rho r^3}$)	Added Damping ($\frac{kg}{s w \rho r^3}$)
0.6	3.66	0.098	1.03	10.2	0.23	10.8	0.42
1.0	9.85	0.265	0.679	10.0	1.34	10.6	1.42
2.0	32.4	0.902	0.587	9.64	0.2	10.4	0.02
3.0	44.7	1.30	0.35	9.8	0.0	10.2	0.0
4.0	74.4	2.00	0.297	10.2	0.0	10.4	0.0
5.0	75.5	2.00	0.174	10.5	0.0	10.3	0.0
6.0	94.6	2.40	0.133	10.6	0.0	10.7	0.0

N=Newtons m=meters s=seconds cm=centimeters kg=kilograms
ρ=density r=radius w=frequency

Table II - Recorded Data - Submerged Cylinder

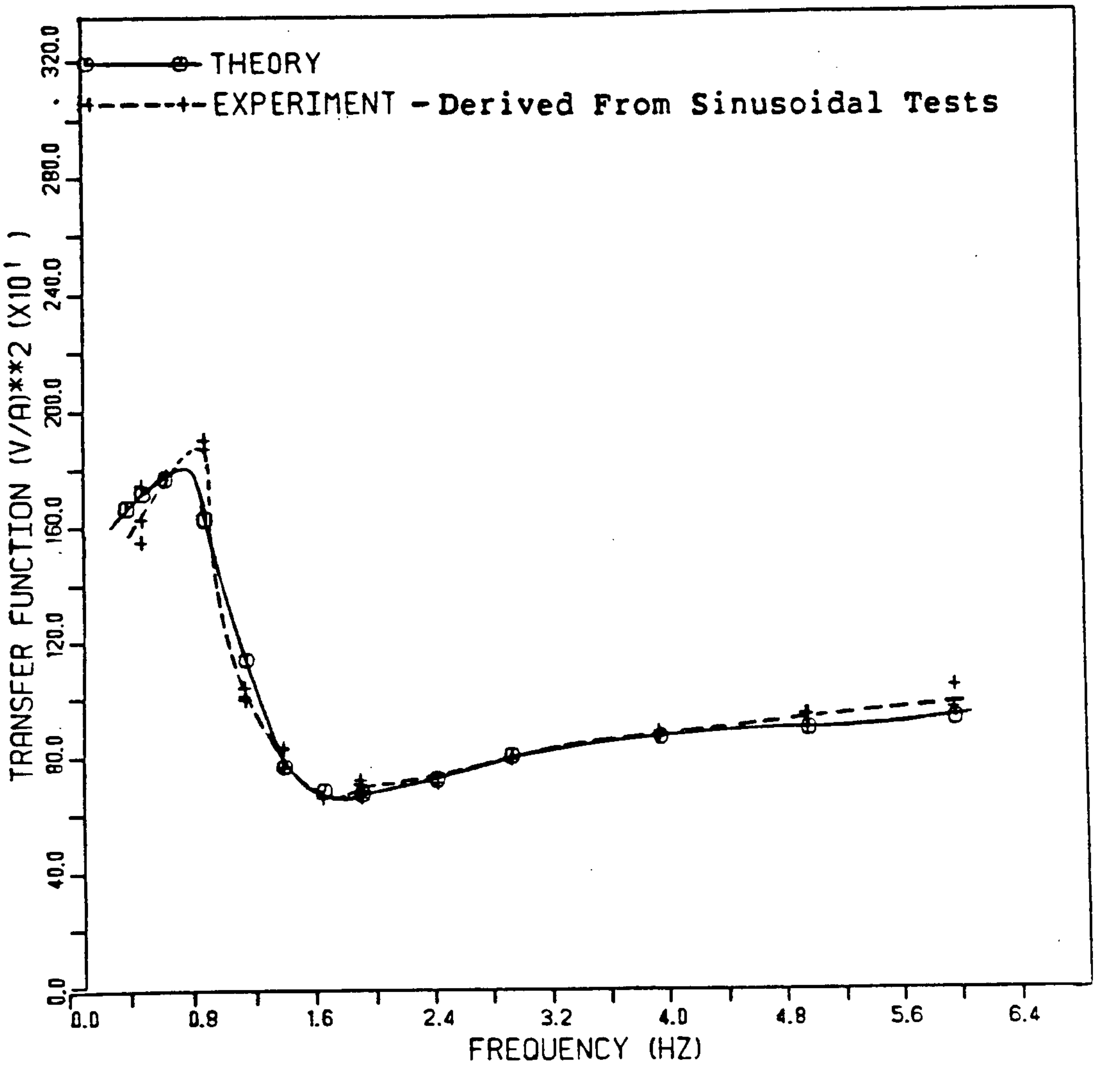

Figure 16 - Transfer Function for the Surface Piercing Cylinder Derived from Sinusoidal Tests

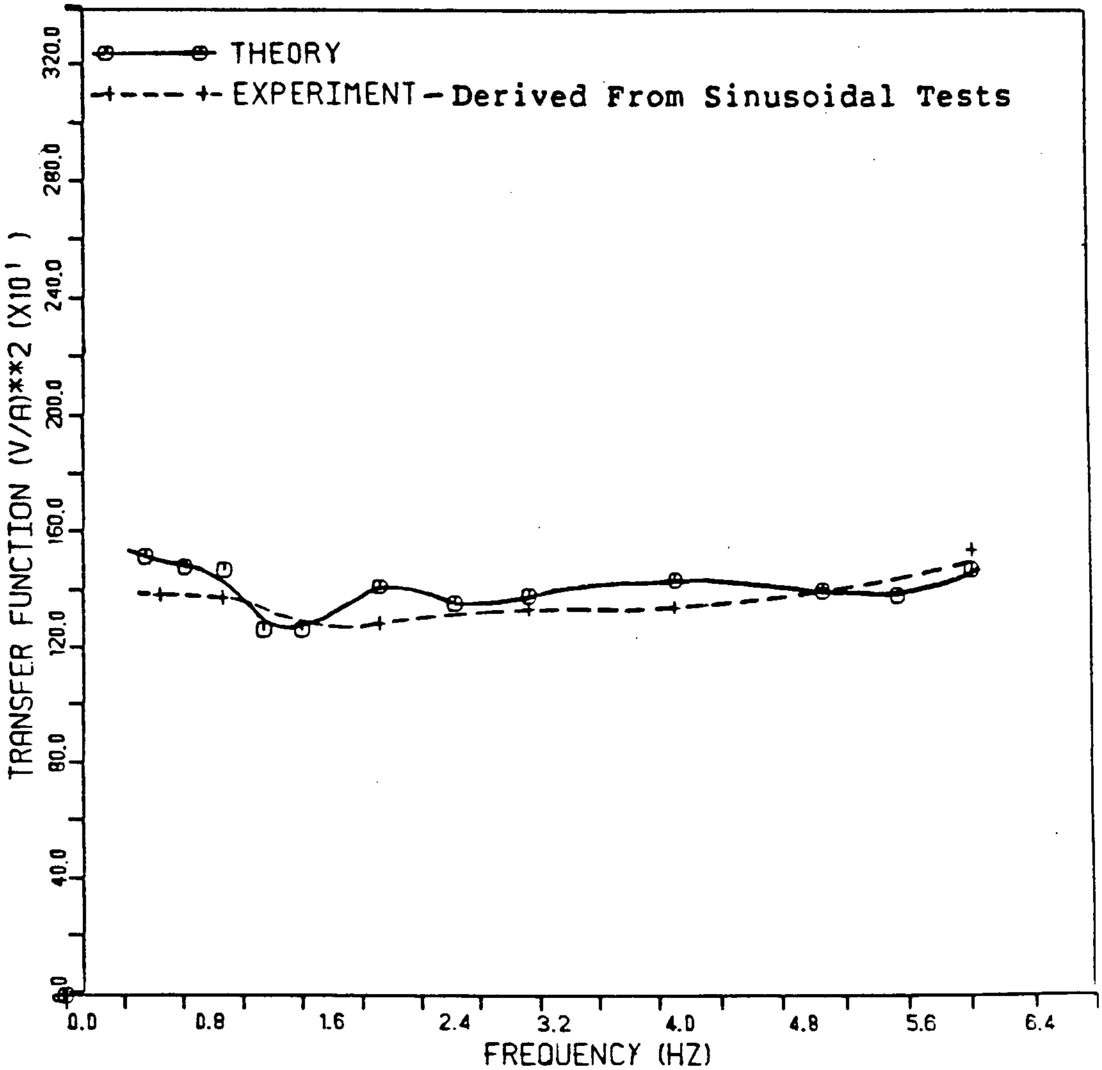

Figure 17 - Transfer Function for the Submerged Cylinder Derived from Sinusoidal Tests

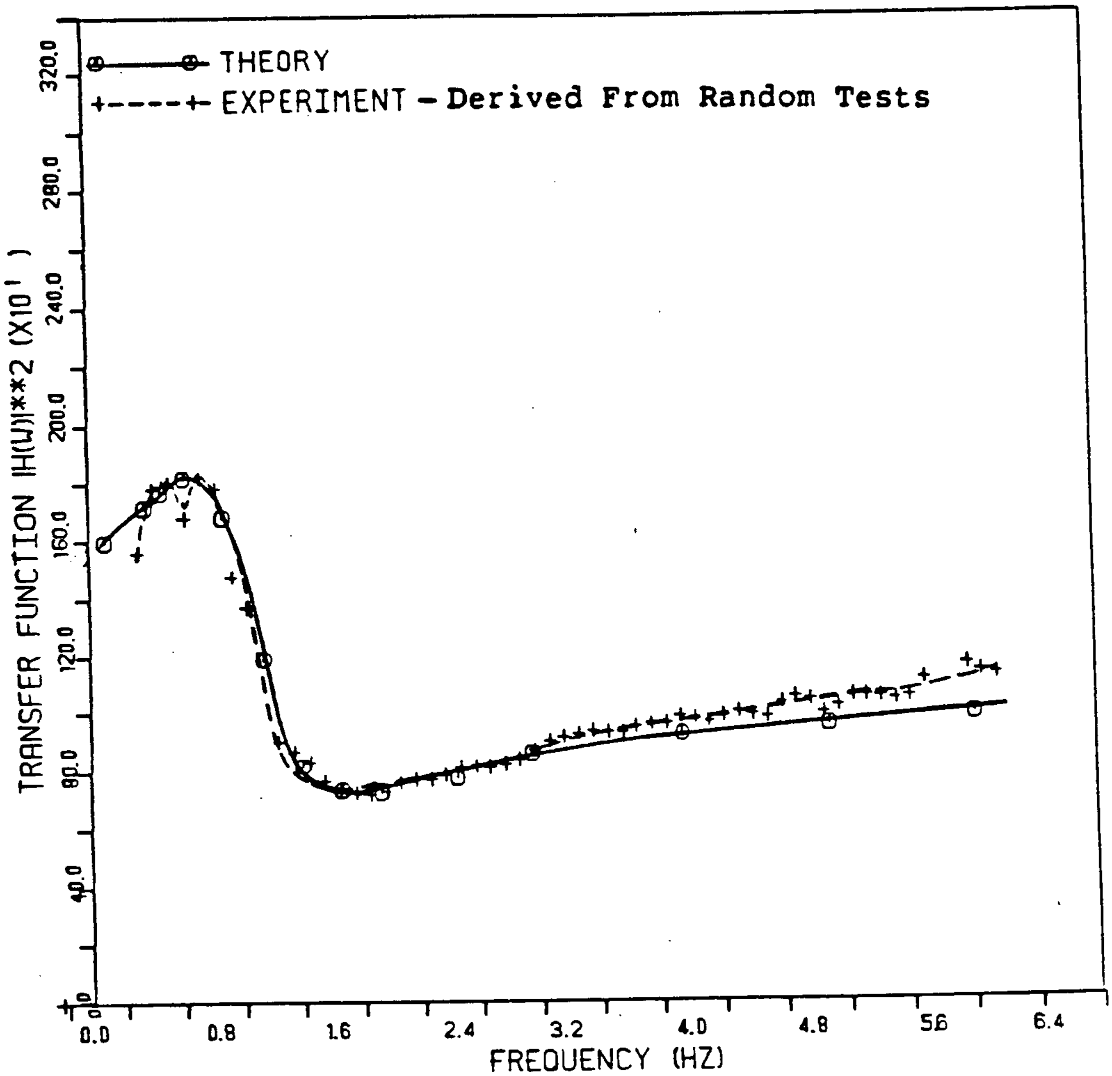

Figure 18 - Transfer Function for Surface Piercing Cylinder: El Centro N-S, 1940

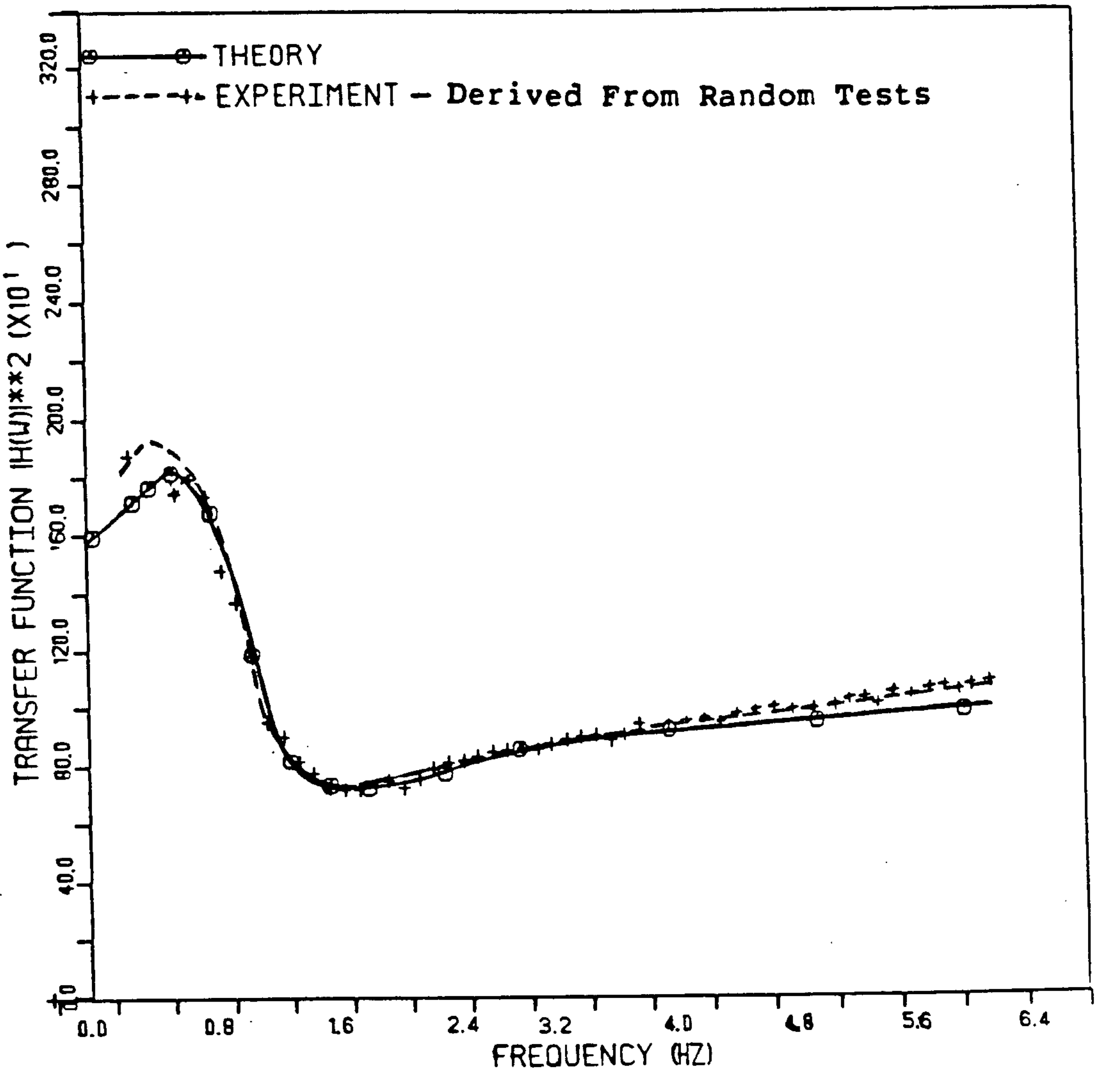

Figure 19 - Transfer Function for Surface Piercing

Cylinder: San Fernando S74W, 1971

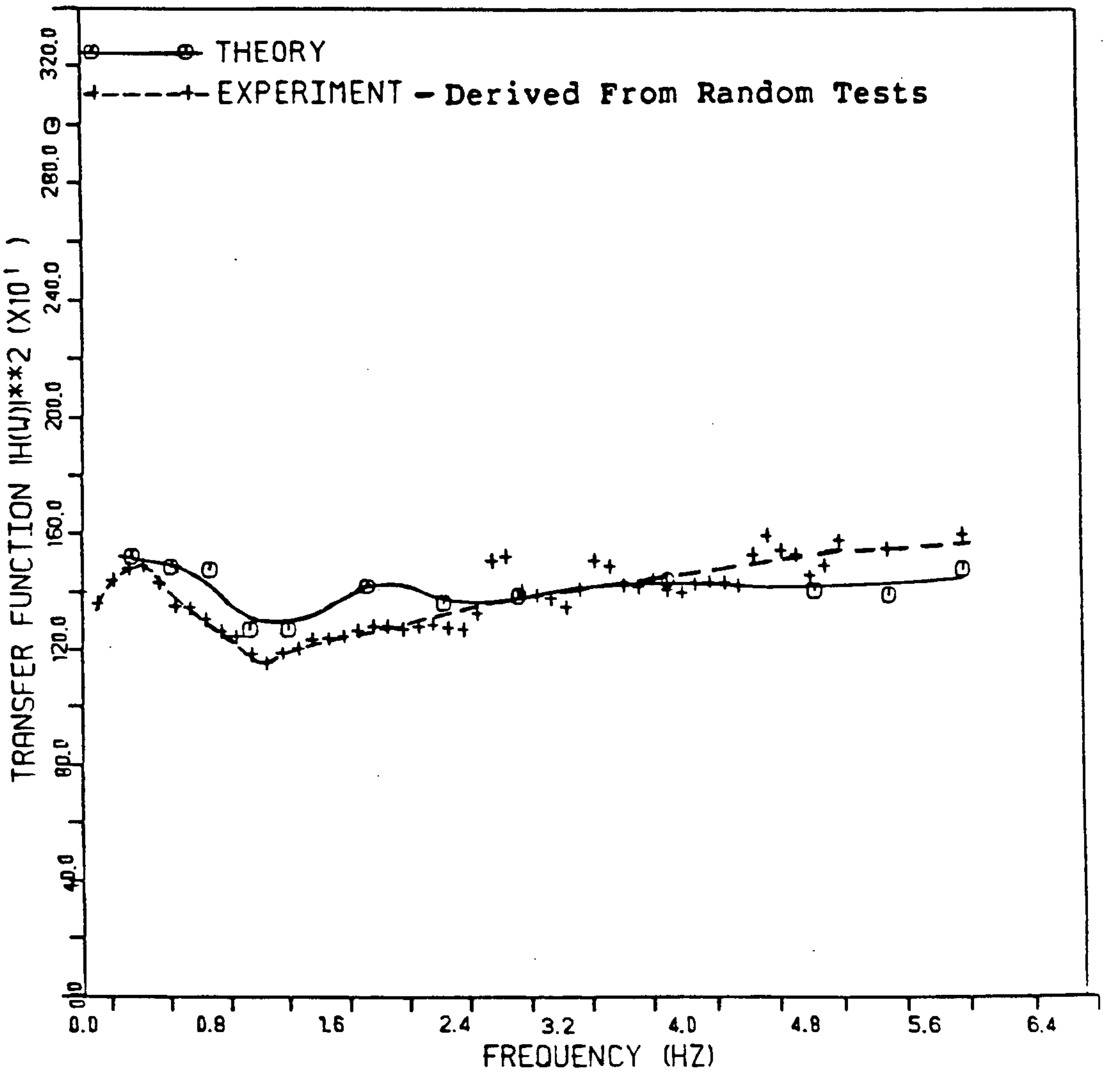

Figure 20 - Transfer Function for Submerged Cylinder: El Centro N-S, 1940

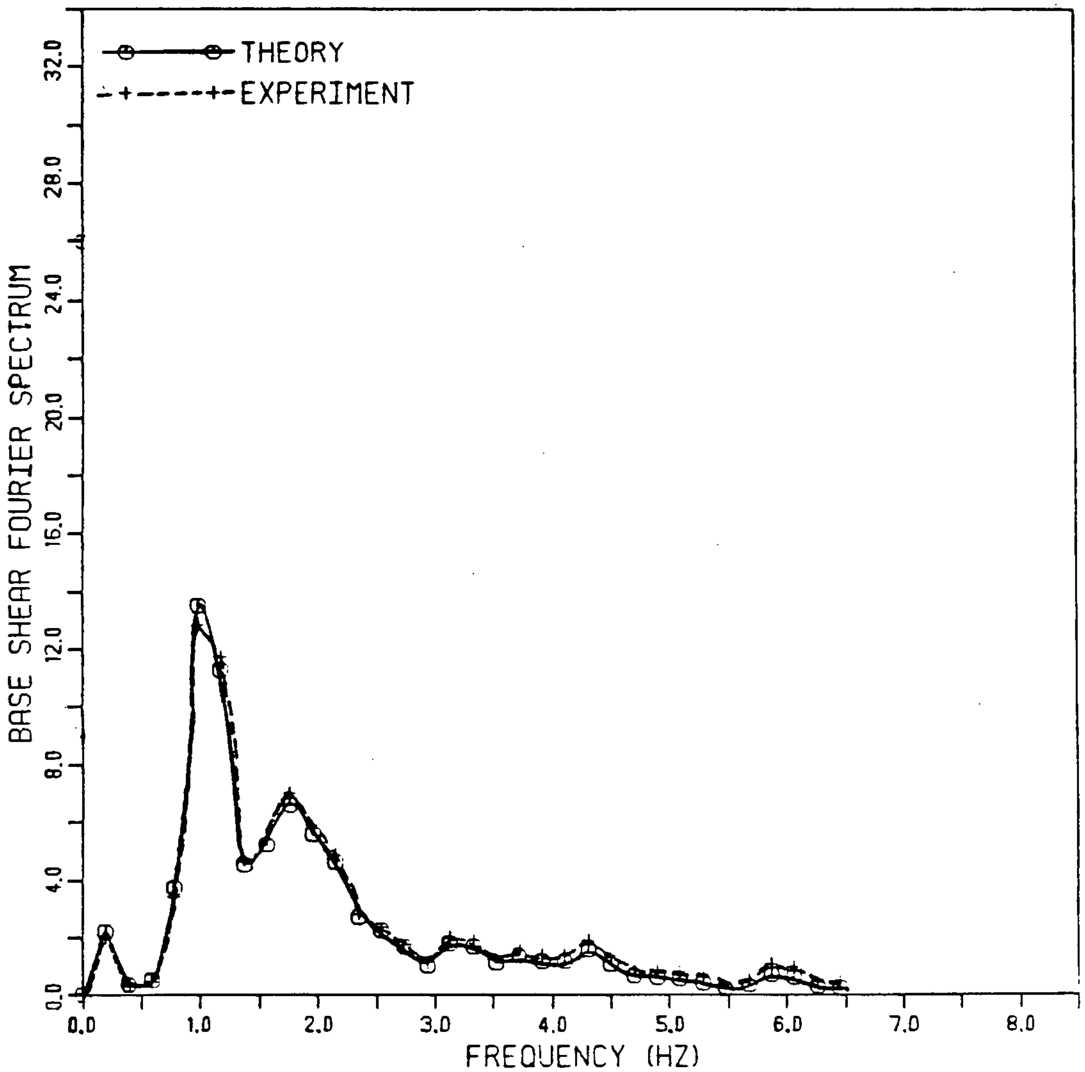

Figure 21 - Frequency Spectrum of Output Base Shear on Surface Piercing Cylinder

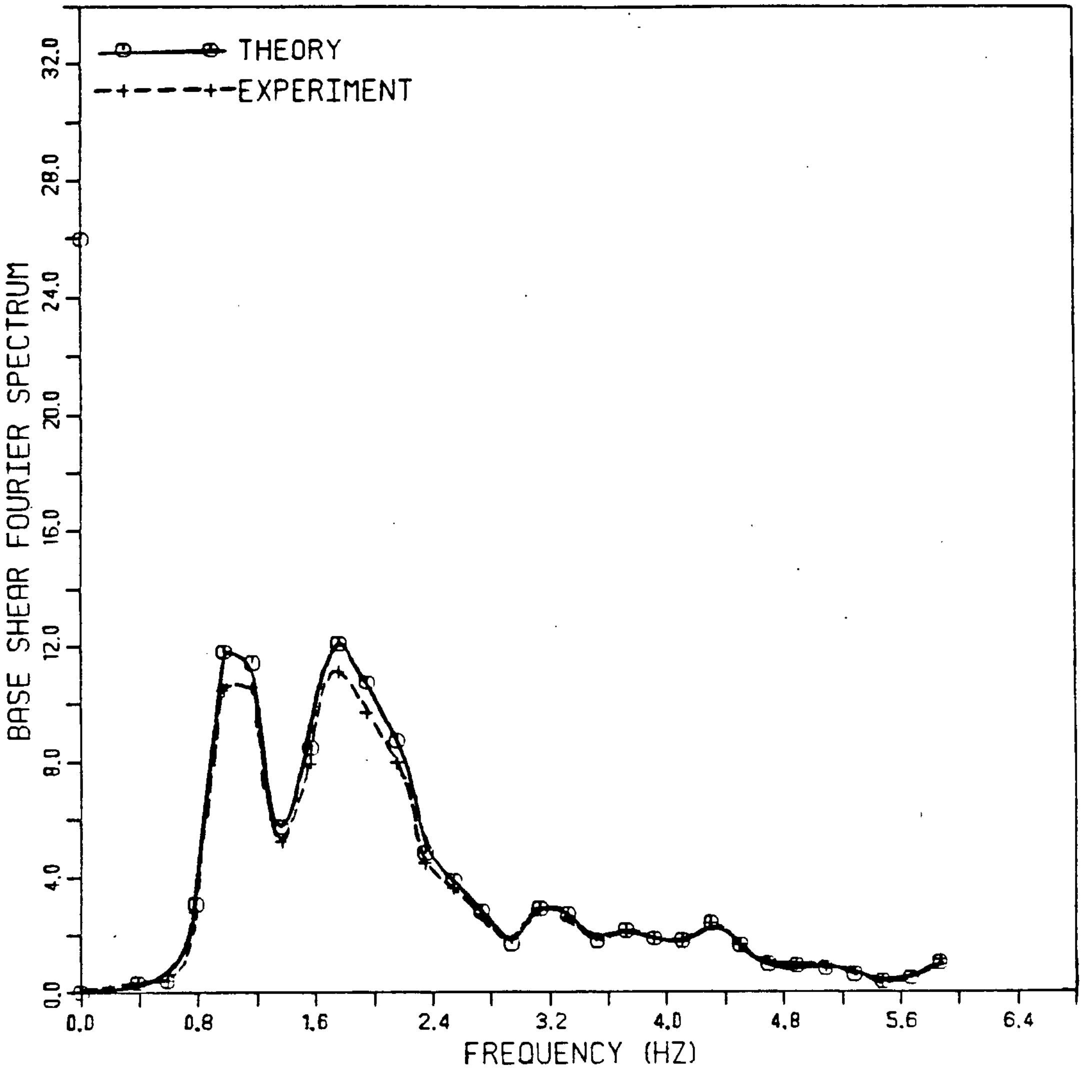

Figure 22 - Frequency Spectrum of Output Base Shear on Submerged Cylinder

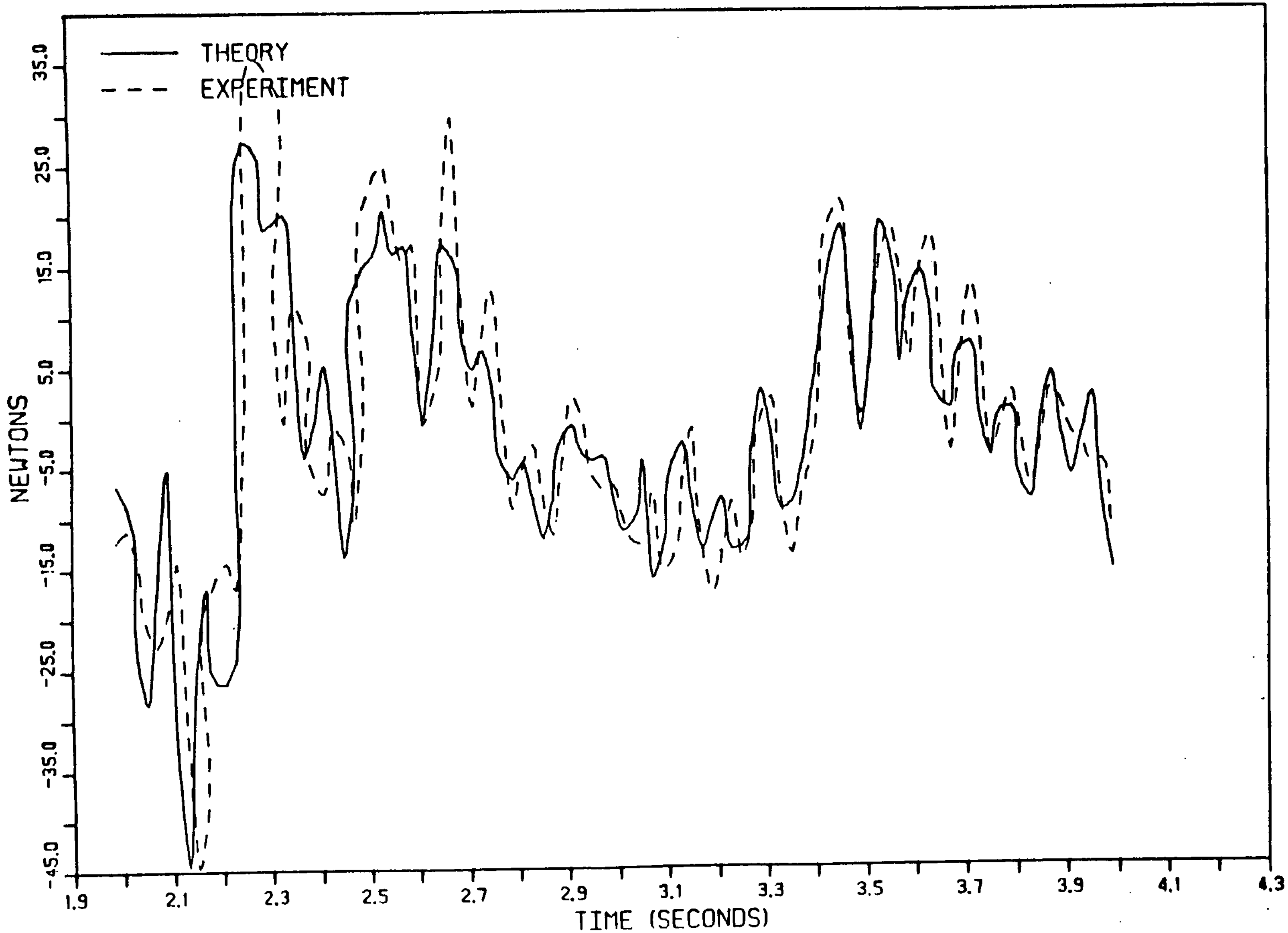

Figure 23 - Comparison of Time Series Output for the El Centro N-S 1940 Earthquake Record

VI. CONCLUSIONS AND RECOMMENDATIONS

The experimental and theoretical values for the added mass, added damping and transfer functions agreed very well. This means that, for structures which meet the characteristics of the Laplace regime (chapter 2), the added mass and damping values calculated from the AXIDIF computer program can be used in design to evaluate the response of a structure as a result of seismic excitation.

For surface piercing structures, the frequency dependence of the added mass and damping due to the production of surface waves is quite significant. In solving for these values theoretically, the full kinematic and dynamic free surface boundary conditions should be included in the solution to account for this frequency dependence.

The submerged structure tests showed that the frequency dependence of the added mass and damping becomes less significant as the structure is submerged below the surface. Solutions which do not include the surface wave effects would probably be quite satisfactory when solving for the fluid forces for most fully submerged structures.

Several areas of investigation are recommended for future study:

- determine added mass and damping values as a function of mode shape for flexible cylinders.

- evaluate fluid forces on structures whose dimensions and motions approach the small body regime, where viscous effects may be important.

- determine experimentally the added mass and damping for structural shapes other than cylinders, possibly to support numerical methods for calculating these parameters.

- study more intensively the effect of submergence on the frequency dependence of the dynamic characteristics.

BIBLIOGRAPHY

1. Bea,R.G., Audibert,J.M., Akkay,M.R., 'Earthquake Response of Offshore Platforms', ASCE Structural Division, Feb. 1979.

2. Bendat,J., Piersol,A., 'Random Data Analysis and Measurement Prodedures', John A. Wiley and Sons, Toronto, 1971.

3. Bury,M.R.C., Domone,P.L., 'The Role of Research in the Design of Concrete Offshore Structures', OTC 1949, 1974.

4. Byrd,R., 'A Study of the Fluid Structure Interaction of Submerged Tanks and Caissons in Earthquakes', EERC - 78/08, May 1978.

5. Chandrasedaran,A., Saini,S.S., Malhatra,M.M., 'Virtual Mass of Submerged Structures',Journal of the Hydraulics Division, ASCE, May 1972.

6. Clough,R.W., 'Effects of Earthquakes on Underwater Structures', Proceedings, Second World Conference on Earthquake Engineering, Roorkee, India, pp 161-171, 1970.

7. Clough,R.W., Penzian,J., 'Dynamics of Structures', McGraw-Hill Inc., New York, 1975.

8. Dong, R.G., 'Effective Mass and Damping of Submerged Structures', U.S. Department of Commerce, Lawrence Livermore Laboratory, Livermore, California, UCRL-52342, April 1978.

9. Dungar,R., Eldred.,P.J., 'The Dynamic Response of Gravity Platforms', Earthquake Engineering and Structural Dynamics, March-April 1978,pp 123-138.

10. Enochson,E., Otnes,R., 'Programming and Analysis for Digital Time Series Data', U.S. Department of Defence, 1968.

11. Finn,L.D., ' A New Deepwater Offshore Platform - The Guyed Tower', OTC 2688, 1976.

12. Gerwick,B., 'Application of Concrete Drilling and Production Caissons to Seismic Areas', OTC 2408, 1975.

13. Gibson,R., Wang,H., 'Added Mass of Pile Groups', ASCE-Waterways, 1977.

14. Helou, Amin Habib, 'Seismic Analysis of Submerged Underwater Oil Storage Tanks', PhD Thesis, North Carolina State University, Raleigh, N.C., 1981.

15. Idress,I.M., Cluff,L.S., Patwardhan,A.S., 'Microzonation of Offshore Areas - An Overview', Microzonation 2nd International Conference, Volume III, 1980.

16. Irani, M.B., 'Finite Element Analysis of Viscous Flow and Rigid Body Interaction', Master's Thesis, University of British Columbia, Vancouver, B.C., 1982.

17. Isaacson, M. de St.Q., 'Interference Effects Between Large Cylinders in Waves', OTC 3067, 1978.

18. Isaacson, M. de St.Q., 'Earthquake Loading of Axisymmetric Offshore Structures', Proceedings, 4th Canadian Conference on Earthquake Engineering, pp 282-287, 1983. see also, Isaacson, M. de St. Q., 'Wave Effects on Fixed and Floating Axisymmetric Structures', Coastal/Ocean Engineering Report, Department of Civil Engineering, University of British Columbia, 1981.

19. Liaw,C.Y., Chopra,A.K., 'Dynamics of Towers Surrounded by Water', EERC - 73/25, 1973.

20. McConnell,K.G., Young,D.F., 'Added Mass of a Sphere in a Bounded Viscous Fluid', ASCE Mechanics Division, August 1965.

21. Morison,J.R., O'Brien,M.P., Johnson,J.W., Schaaf,S.A., 'The Force Exerted by Surface Waves on Piles', Petrol Transactions, AIME, Volume 189, 1950.

22. Nilrat,F., 'Hydrodynamic Pressure and Added Mass for Axisymmetric Bodies', EERC - 80/12, 1980.

23. Penzian,J., Kaul,M., 'Response of Offshore Towers to Strong Motion Earthquakes', Earthquake Engineering and Structural Dynamics 1, July-September 1972.

24. Penzian,J., Van Dao,B., 'Treatment of Non-Linear Drag Forces Acting on Offshore Platforms', EERC - 80/13, 1980.

25. Ruhl,J.A., Berdahl,R.M., 'Forced Vibration Tests of a Deepwater Platform', OTC 3514, 1979.

26. Sarpkaya,T., Isaacson,M. de St.Q., 'Mechanics of Wave Forces on Offshore Structures', Van Nostrand Reinhold Co., Toronto, 1981.

27. Stelson,T.E., Mavis,F.T., 'Virtual Mass and Acceleration in Fluids', ASCE 2870, 1955.

28. Sugiyama,T., Ito,M., 'Dynamic Characteristics of Structures in Water', University of Tokyo Press, 1981.

29. Tanaka,Y., Hamamoto,T., Oshima,M., Ogata,T., 'Dynamics and Behaviors of Offshore Cylindrical Tanks', Japan National Commitee for Theoretical and Applied Mechanics, pp 357, 1980.

30. Taylor, R.E., 'A Review of Hydrodynamic Load Analysis for Submerged Structures Excited by Earthquakes', Engineering Structures, Volume 3, July 1981.

31. Taylor, R.E., Duncan,P.E., 'Fluid-Induced Inertia and Damping in Vibrating Offshore Structures', Applied Ocean Research, Volume 2, 1980.

32. To,N.M., 'The Determination of Structural Dynamic Properties of Three Buildings in Vancouver from Ambient Vibration Surveys', Master's Thesis, University of British Columbia, Vancouver, B.C. 1981.

33. Tung,C.C., 'Hydrodynamic Forces on Submerged Vertical Tanks Under Ground Excitation', Applied Ocean Research, Vol 1, No. 2, pp 75-78, 1979.

34. Van Marche,E. et al, 'Estimation of Dynamic Characteristics of Deep Ocean Tower Structures', Mass. Institute of Technology, Cambridge, Mass., June 1972.

35. Warburton,G.B., Hulton,S.G., 'Dynamic Interaction for Idealized Offshore Structures', Earthquake Engineering and Structural Dynamics - 6, pp 557-567, November-December 1978.

APPENDIX A SOLUTION OF LAPLACE'S EQUATION FOR ADDED MASS AND DAMPNG FOR A CYLINDER USING THE AXIDIF PROGRAM

In this study, the experimental results for added mass and damping were compared with the solution obtained from a wave diffraction theory computer program called AXIDIF [18]. The solution for the forces on submerged structures due to earthquake loading is directly related to the wave loading case as the same added mass and damping values determined by the computer programs are needed to account for the fluid-structure interaction. AXIDIF is for axisymmetric structures only, and is considerably more economical in terms of computer costs than a program for any arbitrarily shaped body.

The theoretical development of the AXIDIF program given here is essentially that of reference [18]. The solution is based on a boundary element method involving an axisymmetric Green's function.

A sinusoidal, unidirectional base motion, Xexp(-iwt) is applied to a rigid axisymmetric structure of cylindrical coordinates, (r,θ,z), where X is a complex amplitude, w is the excitation frequency, r is the radial coordinate , z is the vertical coordinate and θ is the angle measured from the direction of motion. The fluid is considered to be incompressible and inviscid and the flow irrotational. The fluid motion can then be described by the velocity potential satisfying Laplace's equation:

$$\frac{\partial^2\Phi}{\partial r^2} + \frac{1}{r}\frac{\partial\Phi}{\partial r} + \frac{1}{r^2}\frac{\partial^2\Phi}{\partial\theta^2} + \frac{\partial^2\Phi}{\partial z^2} = 0 \tag{A.1}$$

The assumption of incompressible fluid to the case of a body vibrating in water is discussed at some length by Liaw and Chopra [19]. For most structure dimensions and frequencies of vibration this assumption is quite valid but for some cases, water compressibility should be considered.

With the assumption of small amplitude motion and the fluid assumptions discussed in chapter 2, the usual linearized boundary conditions are applied to the differential equation. The relevent boundary conditions are:

1. $$\frac{\partial\Phi}{\partial z}(r,0,\theta,t)=0 \tag{A.1a}$$

   defines the velocity condition normal to the ocean floor at z=0

2. $$\frac{\partial\Phi}{\partial n}(R,z,\theta,t)= -iw\cos\alpha\cos\theta \tag{A.1b}$$

   specifies that the fluid particle motion and the motion of the structure is the same at the structure boundary; n is the direction normal to the structure surface and α is the direction of n in relation to the horizontal axis.

3. $$\frac{\partial^2\Phi}{\partial t^2}(r,H,\theta,t)=-g\frac{\partial\Phi}{\partial z}(r,H,\theta,t) \tag{A.1c}$$

   describes a linearized free surface condition including dynamic and kinematic boundary conditions; H=total depth of water.

4. $$\frac{\partial\Phi}{\partial\theta}(r,z,O,t)=\frac{\partial\Phi}{\partial\theta}(r,z,\pi,t) \tag{A.1d}$$

stipulates symmetry about θ=0 plane

The velocity potential is harmonic and proportional to the amplitude of motion, ΦXexp(-iwt). In the boundary integral method, the unknown potential, Φ(x), at the general point, x=(r,θ,z), is represented as due to a source distribution over the structure's surface S_0, and is thus expressed as:

$$\Phi(x) = \frac{1}{4\pi} \int_{S_o} f(x)G(x,y)dS \tag{A.2}$$

Here, f(x) is a source strength distribution function, G(x,y) is a Green's function for the general point x due to a source of unit strength at y, and the integration is carried out for all points y over S_0. G is itself chosen to satisfy the Laplace equation, the seabed and linearized free surface boundary conditions, and the radiation condition. This ensures that Φ also satisfies these equations, and it remains for f to be chosen so as to ensure that the boundary condition on the structure surface is satisfied.

Boundary condition A1.b equating the fluid velocity normal to the structure surface to the velocity of the structure surface, together with equation A.2 gives rise to a surface integral equation for f:

$$-\frac{1}{2} f(x) + \frac{1}{4\pi} \int_{S_o} f(y) \frac{\partial G}{\partial n}(x,y)\,dS = -iw \cos\alpha \cos\theta \tag{A.3}$$

Here, n is measured from the point x, and the integration is carried out over the point y. In equation A.3, x lies on the structure surface and may be defined by the coordinates (s,θ), where s is the surface coordinate and y may be defined by corresponding coordinates (s',θ').

Because of the structure's axisymmetry, the functions Φ, f and G for points on the structure surface may be expanded as Fourier series:

$$\Phi(s,\theta) = \sum_{m=1}^{\infty} \Phi_m(s) \cos m\theta \tag{A.4}$$

$$f(s,\theta) = \sum_{m=1}^{\infty} f_m(s) \cos m\theta \tag{A.5}$$

$$G(s,\theta,s',\theta') = \sum_{m=1}^{\infty} G_m(s,s') \cos m(\theta-\theta') \tag{A.6}$$

and only the terms corresponding to m=1 will be required here. Substituting equations A.5 and A.6 into A.3, algebraic manipulation yields a set of line integral equations, of which the equation corresponding to m=1 is:

$$-f_1(s) + \frac{1}{2} \int_{S_o} f_1(s') R(s') \frac{\partial G_1}{\partial n}(s,s')\,ds' = 2iw\cos\alpha \tag{A.7}$$

Here, s_0 is the structure's entire contour described by s, and $R(s')$ is the structure's radius at s'.

In a numerical solution to equation A.7, the contour s_0 is discretized into N short segments with the function f_1 taken to be uniform over each segment, and equation A.7 is applied at the centre of each segment. Thus equation A.7 may be approximated by a matrix equation:

$$\sum_{k=1}^{N} A_{jk} f_k^{(1)} = -2iw\cos\alpha \qquad \text{for } j=1,2,\ldots N \tag{A.8}$$

where $f_k^{(1)}$ denotes $f_1(s_k)$. Expressions for the matrix coefficients A_{jk} are given by Isaacson [18]. Once the source strengths $f_k^{(1)}$are determined, the potential itself can be obtained by a discretized form of equation A.2. The necessary Fourier coefficient Φ_1 at the j-th segment centre can be approximated as:

$$\Phi_1(s_j) = 1/2 \sum_{k=1}^{N} f_k^{(1)} C_{jk} \qquad \text{for } j=1,2,\ldots N \tag{A.9}$$

Once more, Isaacson [18], provides expressions for the coeffients C_{jk}.

Now that the potential function Φ_1 is known, the hydrodynamic loads on the structure may be evaluated.

The hydrodynamic pressure p acting on the structure surface is given by the linearized Bernoulli equation, $p = iw\rho\ \Phi \exp(-iwt)$, where ρ is the fluid density. Thus the horizontal force $F_1^{(f)} \exp(-iwt)$ and overturning moment $F_2^{(f)} \exp(-iwt)$ due to the fluid may be expressed as:

$$F_j^{(f)} = -iw\rho \int_S \Phi n_j ds\ , \qquad \text{for } j=1,2 \tag{A.10}$$

where $n_1 = \cos\alpha\cos\theta$

$n_2 = z\cos\alpha\cos\theta - r\sin\alpha\cos\alpha$

Substituting the Fourier expansion of Φ, equation A.5, and integrating with respect to θ, we obtain

$$F_j^{(f)} = -\pi iw\rho \sum_{k=1}^{N} L_k r_k n_{jk} \Phi_1(s_k) \qquad \text{for } j=1,2 \tag{A.11}$$

where L_k is the length of the k-th segment, and

$n_{1k} = \cos\alpha_k$

$n_{2k} = z_k\cos(\alpha_k) - r_k\sin(\alpha_k)$

The fluid forces $F_j^{(f)}$ are conveniently expressed in terms of added masses m_{aj}, and damping coefficients λ_j, by taking:

$$F_j^{(f)} = w^2 m_{aj} + iw\lambda_j \tag{A.12}$$

in which m_{aj} and λ_j may be retrieved by separating the real and imaginary parts of $F_j^{(f)}$. It is emphasized that m_{aj} and

λ_j are frequency dependent variables.

Many authors [4,19,4 and 33], set the free surface boundary condition, equation A.1c, equal to 0:

$$\frac{\partial^2 \Phi(r,H,\theta,t)}{\partial t^2} = 0 \qquad \text{(A.13)}$$

This greatly simplifies the solution but neglects any surface wave effects and results in the solution being independent of the excitation frequency. These effects can be important for some structures as discussed in chapter 5.

APPENDIX B MEASUREMENT AND ANALYSIS OF DATA

1. MEASUREMENT APPARATUS

A. Base Acceleration

The measurement of the base input to the cylinder was made with an accelerometer fastened directly to the shaking table. A Kistler MD 305A 50g accelerometer, in conjunction with a servoamplifier, was used for this purpose.

B. Base Displacement

The displacement of the table (and hence the base of the cylinder) was recorded as a check on the acceleration measurements. These measurements were taken with the LVDT, which is attached permanently to the arm of the hydraulic jack exciting the table.

C. Base Shear

The shear developed at the base of the cylinder was measured using strain gauges. Four strain gauges were used on the shaft of the model arranged in a full Wheatstone Bridge (Figure 24). The bridge was set up to measure the difference between the average strain at the top of the shaft and at the bottom of the shaft. The base shear is directly proportional to this difference in strain:

$$V = \frac{\epsilon EI}{yH} \qquad (B.1)$$

where:
V = base shear
E = modulus of elasticity of the shaft (steel in this case)
I = moment of inertia of shaft
ϵ = difference between the average strain at the top and at the bottom of shaft
y = distance from neutral axis to outer fiber of shaft
H = height of shaft between strain gauges

The constant EI/yH was evaluated by a load calibration test of the model prior to conducting the experiments; in this test, ϵ was measured for known values of V and EL/yH was calculated from B.1.

The base shears and thus the strain gauge output voltages varied over a wide range of values, being very small at low loads to quite large at high load levels. As a result, it was necessary to use a variable amplifier to boost and condition the data signals to a suitable level for recording on the PDP-11 mini computer.

2. DATA COLLECTION

The experiments were carried out in the Earthquake Simulation Laboratory of the Department of Civil Engineering at the University of British Columbia. This facility is equipped with a PDP-11 mini computer with disc drive, backed by an RT-11 operating system. It is capable of handling 17 channels of input; the tests required only three. Each channel is equipped with a variable amplifier and a variable filter to bring the generated signals up to recordable level.

The data for the base shear V, base acceleration a, and base displacement X, were recorded onto a floppy disc. Each sinusoidal test was recorded over a ten second period at a sampling rate of 100 samples per second. To aid in smoothing the data, the filters were set at cutoff values of at least twice the test frequency.

A typical set of results from the sinusoidal tests is shown in Figure 25. As can be seen the plots are not pure sinusoids. This was caused by imperfections in the shaking table system, which produce small, high frequency vibrations other than those desired in the test. This problem cannot be corrected and must be compensated for in the analysis by using Fourier spectra as described in the next section.

The random tests were recorded in the same manner. Real earthquake records were fed into the table through the PDP-11 system to provide the random excitation. Figure 26 is an example of the base shear, acceleration, and displacement recorded during a test of the surface piercing cylinder using the 1940 N-S El Centro record. The data for the random tests were filtered at 50 Hz to eliminate high frequency noise from the system.

3. ANALYSIS OF DATA

A. Sinusoidal Tests

The sinusoidal tests provided information on the amplitudes of the base shear V, and the base acceleration a, and the phase shift ϕ, between these variables. The table displacement X, was used as a check on the acceleration through the simple harmonic relation $a=-w^2X$. The added mass and damping were then derived from this information as discussed in Chapter 2.

If the data were purely sinuoidal it would be quite easy to determine the above values; however, as can be seen in Figure 25, this was not the case. To isolate the peak value at the test frequency from the data, a Fourier analysis was used to produce Fourier spectra. Fourier amplitude and phase spectra were produced for the base shear and the base acceleration of each test (see example, Figure 27). The required amplitudes, V and a, and the phase shift, ϕ, were then taken directly from the spectra, the phase shift being the difference between the phase values of V(t) and a(t).

A given record in the time domain:

$$x(t)=X_0\cos(w_0t+\theta_0) = X_0\exp(i(w_0t+\theta_0)) \tag{B.2}$$

can be transformed into the frequency domain by taking its Fourier transform:

$$F(w)= \int x(t)\exp(-iwt)dt = X_0\exp(i\theta_0)\int_{-\infty}^{\infty}\exp(i(w_0-w)t)dt \tag{B.3}$$

This may be written as:

$$F(w) = X_o \exp(i\theta_o)\,\delta(w-w_o) \quad \text{where} \quad \int_{-\infty}^{\infty} \exp(iwt)\,dt = \delta(w) \tag{B.4}$$

which on expansion becomes:

$$F(w) = X_o \cos\theta_o \delta(w-w_o) + X_o\, i \sin\theta_o \delta(w-w_o) \tag{B.5}$$

Then the Fourier Amplitude $= \sqrt{Re^2+Im^2} = |F(w)|$

$$= X_o\sqrt{\cos^2\theta_o + \sin^2\theta_o}\;\delta(w-w_o) \qquad = X_o\,\delta(w-w_o) \tag{B.6}$$

and the phase angle $= \theta = \tan^{-1}\dfrac{Im}{Re} = \tan^{-1}\dfrac{X_o \sin\theta\,\delta(w-w_o)}{X_o\cos\theta\,\delta(w-w_o)}$

$$= \tan^{-1}(\tan\theta_o) = \theta_o \tag{B.7}$$

This analysis is true for each frequency component, $A_n \cos(w_n t + \theta_n)$ in the data.

B. Random Tests

Random tests were performed in which the cylinder base shears and accelerations were measured when using the El Centro 1940 N-S and the San Fernando S74W, 1971 earthquakes as the input excitation. The parameter of interest here was the frequency transfer function relating the input acceleration and the output base shear.

Assuming a stationary process, which may be taken as reasonable for at least part of the earthquake records, the frequency transfer function can be derived from the spectral densities of the input and output records [7]:

$$\frac{Sv}{Sa} = |H(w)|^2 \tag{B.8}$$

where:

Sv is the spectral density of the output base shear
Sa is the spectral density of the input acceleration record
$|H(w)|$ is the amplitude of the frequency transfer function

The base shear V(t), and the acceleration a(t), data were run through a Fast Fourier Transform program (FFT) from which the power spectral densities were calculated (see Figure 28). The graph of the ratio of the power spectral density values, $|H(w)|^2$, at each frequency produces the frequency transfer function.

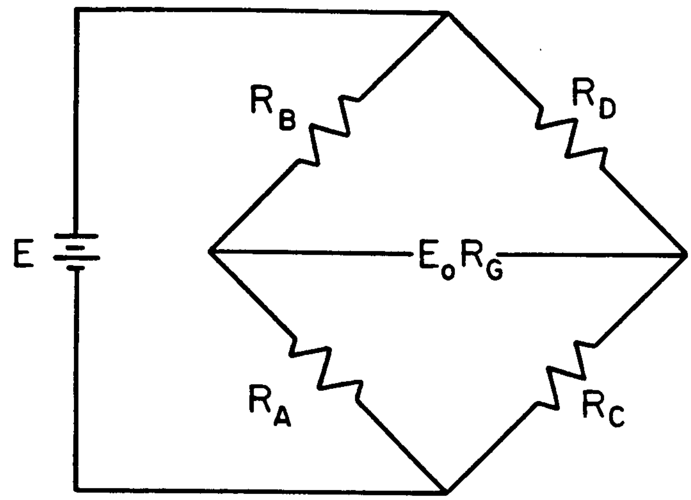

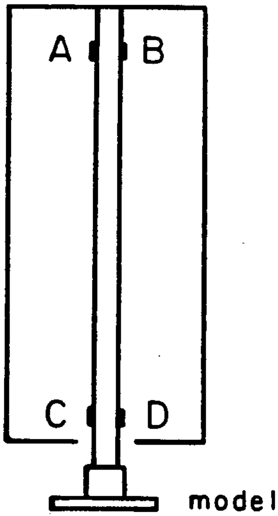

$$E_o = \frac{E R_G}{4(R+R_G)}\left[\frac{\Delta R_B}{R_B} - \frac{\Delta R_D}{R_D} + \frac{\Delta R_C}{R_C} - \frac{\Delta R_A}{R_A}\right]$$

$$R_A = R_B = R_C = R_D \qquad \epsilon F = \frac{\Delta R}{R}$$

$$\epsilon = \frac{2E_o(R+R_G)}{E R_G F}$$

ϵ = strain
E_o = measured voltage
R = strain gauge resistance
R_G = galvanometer resistance
E = excitation voltage
F = gauge factor

Figure 24 - Wheatstone Bridge - Strain Gauge Configuration

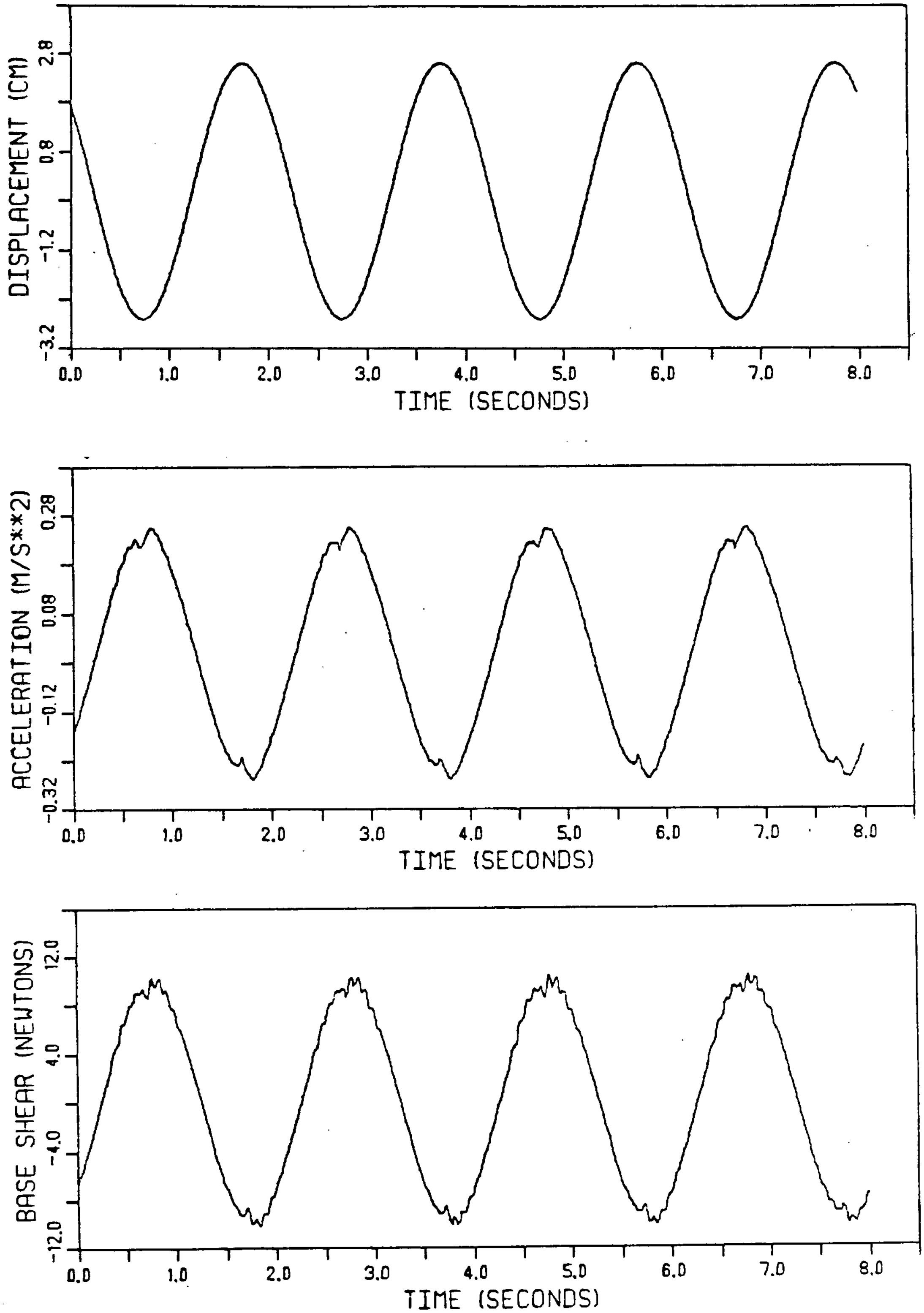

Figure 25 - Example of Data From Sinusoidal Tests

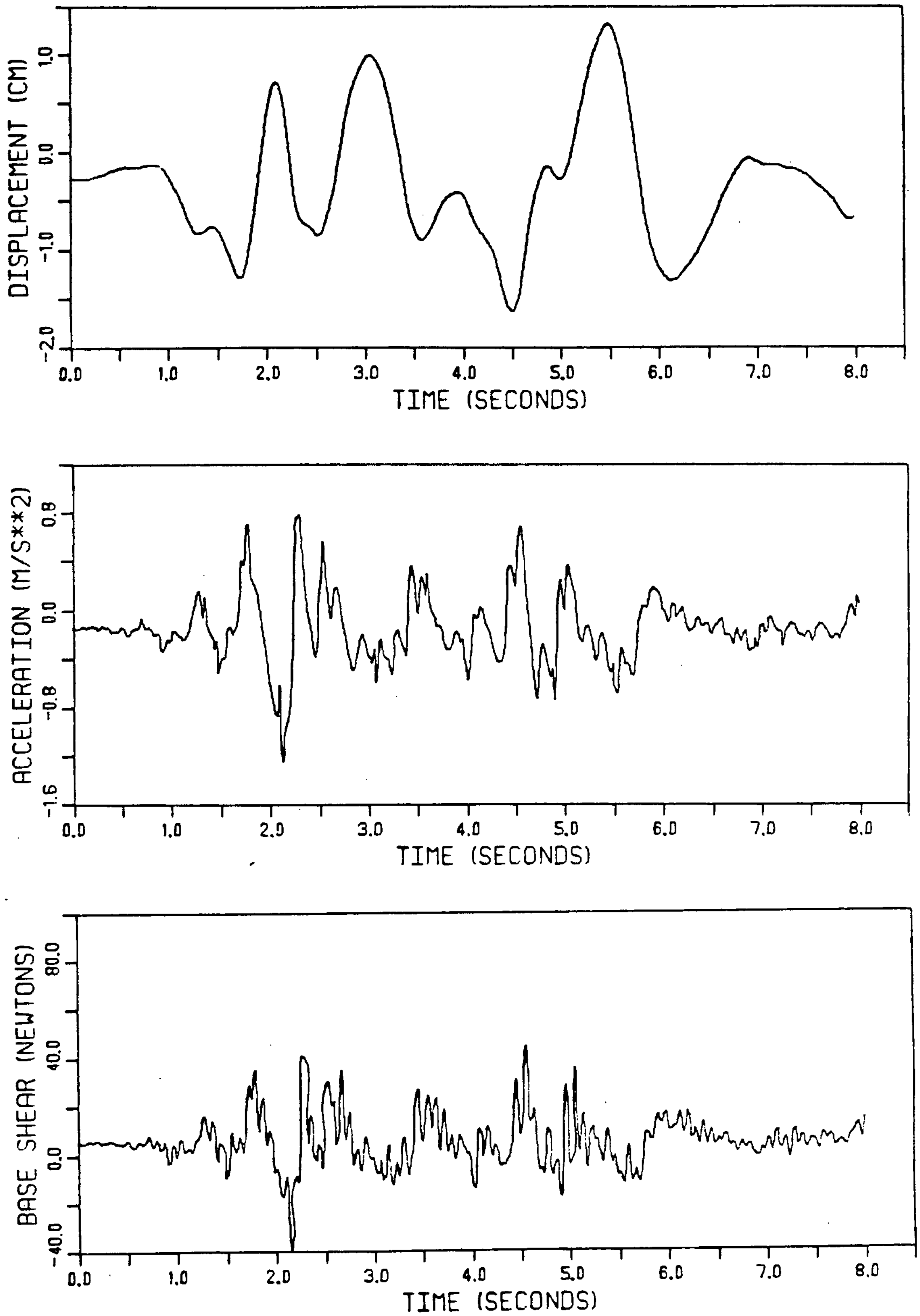

Figure 26 - Example of Data From Random Earthquake Tests

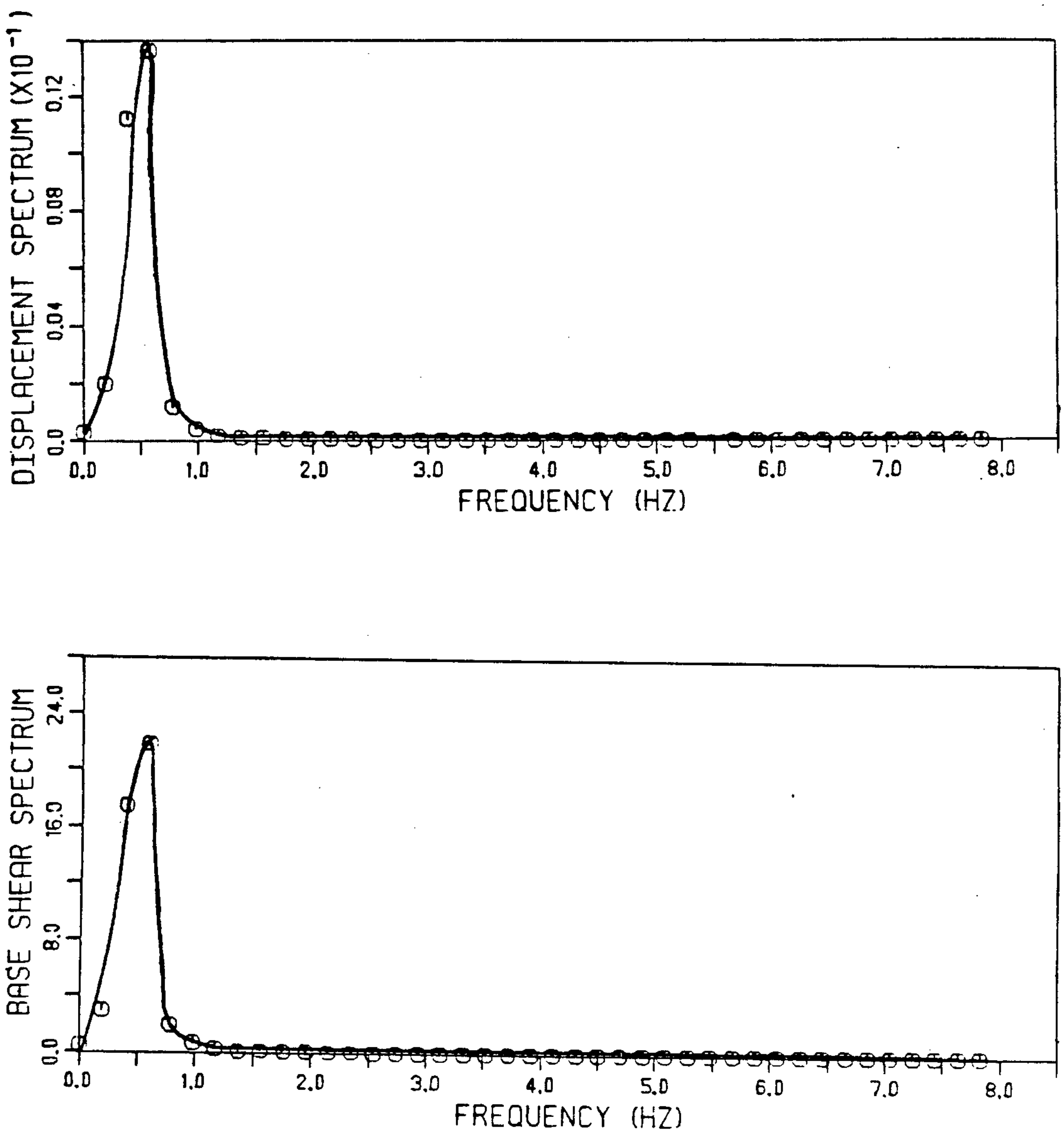

Figure 27 - Fourier Amplitude Spectra for Sinusoidal Data of Base Shear and Acceleration

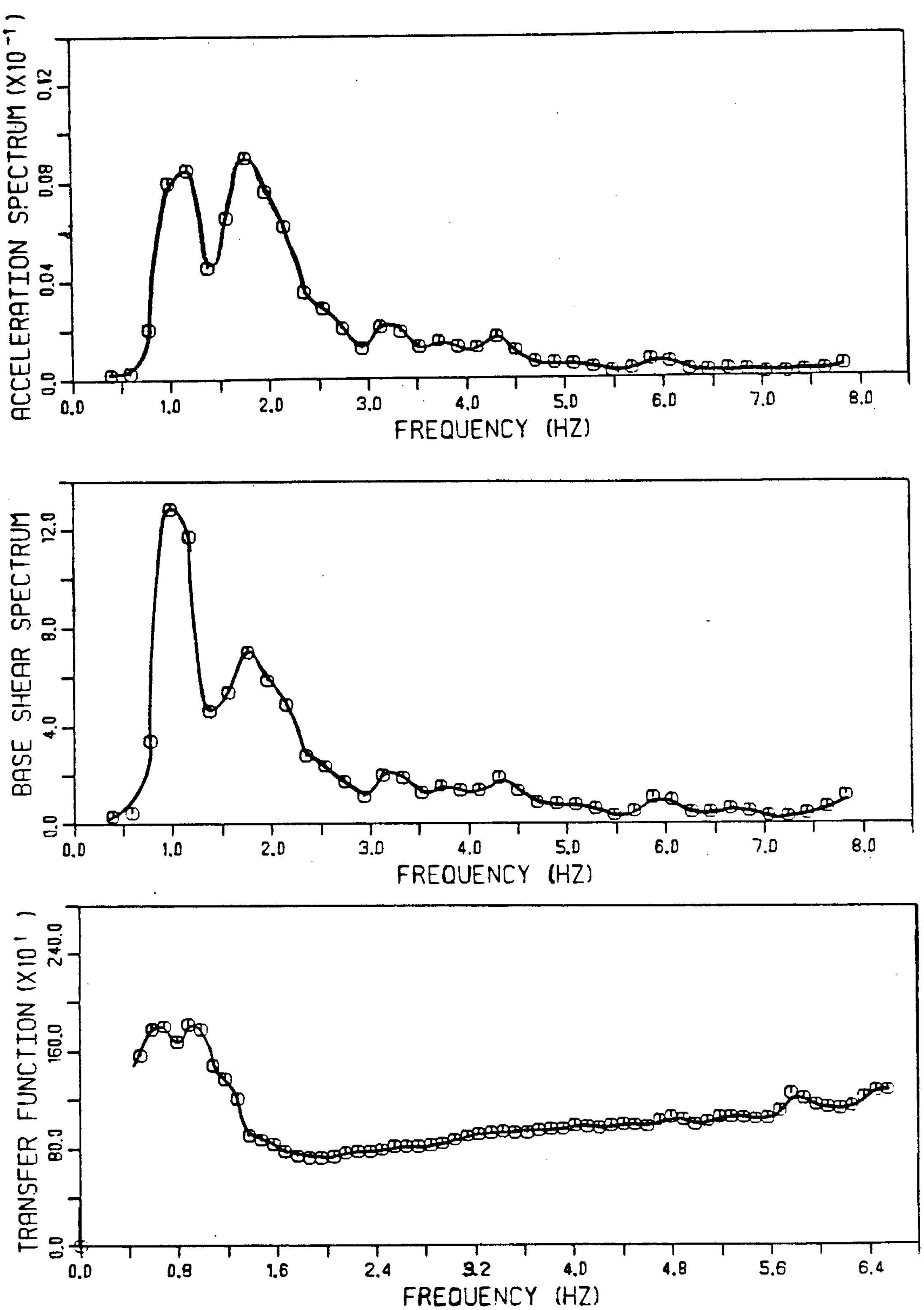

Figure 28 - Spectras of Base Shear and Acceleration and Transfer Function Derived from them